Inorg. Chem. **2003**, *42*, 1807–1824

Copper(I)–Dioxygen Reactivity of $[(L)Cu^{I}]^{+}$ (L = Tris(2-pyridylmethyl)amine): Kinetic/Thermodynamic and Spectroscopic Studies Concerning the Formation of $Cu–O_2$ and $Cu_2–O_2$ Adducts as a Function of Solvent Medium and 4-Pyridyl Ligand Substituent Variations

Christiana Xin Zhang,[†] Susan Kaderli,[‡] Miguel Costas,[‡] Eun-il Kim,[†] Yorck-Michael Neuhold,[‡] Kenneth D. Karlin,*[,†] and Andreas D. Zuberbühler*[,‡]

Department of Chemistry, The Johns Hopkins University, Baltimore, Maryland 21218, and Department of Chemistry, University of Basel, CH-4056 Basel, Switzerland

Received September 18, 2002

The kinetic and thermodynamic behavior of O_2-binding to Cu(I) complexes can provide fundamental understanding of copper(I)/dioxygen chemistry, which is of interest in chemical and biological systems. Here we report stopped-flow kinetic investigations of the oxygenation reactions of a series of tetradentate copper(I) complexes $[(L^R)Cu^I(MeCN)]^+$ (**1**$^{\mathbf{R}}$, R = H, Me, tBu, MeO, Me_2N) in propionitrile (EtCN), tetrahydrofuran (THF), and acetone. The syntheses of 4-pyridyl substituted tris(2-pyridylmethyl)amine ligands (L^R) and copper(I) complexes are detailed. Variations of ligand electronic properties are manifested in the electrochemistry of **1**$^{\mathbf{R}}$ and ν(CO) of $[(L^R)Cu^I–CO]^+$ complexes. The kinetic studies in EtCN and THF show that the O_2-reactions of **1**$^{\mathbf{R}}$ follow the reaction mechanism established for oxygenation of **1**$^{\mathbf{H}}$ in EtCN (*J. Am. Chem. Soc.* **1993**, *115*, 9506), involving reversible formation (k_1/k_{-1}) of $[(L^R)Cu^{II}(O_2^{-})]^+$ (**2**$^{\mathbf{R}}$), which further reacts (k_2/k_{-2}) with **1**$^{\mathbf{R}}$ to form the 2:1 Cu_2O_2 complex $[\{(L^R)Cu^{II}\}_2(O_2^{2-})]^{2+}$ (**3**$^{\mathbf{R}}$). In EtCN, the rate constants for formation of **2**$^{\mathbf{R}}$ (k_1) are not dramatically affected by the ligand electronic variations. For R = Me and tBu, the kinetic and thermodynamic parameters are very similar to those of the parent complex (**1**$^{\mathbf{H}}$); e.g., k_1 is in the range 1.2×10^4 to 3.1×10^4 M^{-1} s^{-1} at 183 K. With the stronger donors R = MeO and Me_2N, more significant effects were observed, with the expected increase in thermodynamic stability of resultant **2**$^{\mathbf{R}}$ and **3**$^{\mathbf{R}}$ complexes, and decreased dissociation rates. The modest ligand electronic effects manifested in EtCN are due to the competitive binding of solvent and dioxygen to the copper centers. In THF, a weakly coordinating solvent, the formation rate for **2**$^{\mathbf{H}}$ is much faster ($\geq$100 times) than that in EtCN, and the thermodynamic stabilities of both the 1:1 (K_1) and 2:1 ($\beta = K_1K_2$) copper–dioxygen species are much higher than those in EtCN (e.g., for **2**$^{\mathbf{H}}$, $\Delta H°$ (K_1) = –41 kJ mol^{-1} in THF versus –29.8 kJ mol^{-1} in EtCN; for **3**$^{\mathbf{H}}$, $\Delta H°$ (β) = –94 kJ mol^{-1} in THF versus –77 kJ mol^{-1} in EtCN). In addition, a more significant ligand electronic effect is seen for the oxygenation reactions of **1**$^{\mathbf{MeO}}$ in THF compared to that in EtCN; the thermal stability of superoxo- and peroxocopper complexes are considerably enhanced using L^{MeO} compared to L^H. In acetone as solvent, a different reaction mechanism involving dimeric copper(I) species $[(L^R)_2Cu^I_2]^{2+}$ is proposed for the oxygenation reactions, supported by kinetic analyses, electrical conductivity measurements, and variable-temperature NMR spectroscopic studies. The present study is the first systematic study investigating both solvent medium and ligand electronic effects in reactions forming copper–dioxygen adducts.

Introduction

Much of the inspiration for the current research in synthetic copper$-O_2$ chemistry[1–7] comes from a bioinorganic perspective and the extensive occurrence of copper-containing proteins which process dioxygen.[2,8,9] X-ray structures of

* To whom correspondence should be addressed.
[†] Johns Hopkins University.
[‡] University of Basel.

(1) Kitajima, N.; Moro-oka, Y. *Chem. Rev.* **1994**, *94*, 737−757.
(2) Karlin, K. D.; Zuberbühler, A. D. In *Bioinorganic Catalysis: Second Edition, Revised and Expanded*; Reedijk, J., Bouwman, E., Eds.; Marcel Dekker: New York, 1999; pp 469−534.
(3) Schindler, S. *Eur. J. Inorg. Chem.* **2000**, 2311−2326.

10.1021/ic0205684 CCC: $25.00
Published on Web 02/12/2003

blood-dioxygen carrier hemocyanins (i.e., in arthropods and mollusks)[8,10,11] reveal the presence of side-on μ-η^2:η^2-peroxodicopper(II) moieties where each copper ion binds three nitrogen ligands from histidine imidazole groups. Spectroscopic comparisons suggest that this binding mode occurs also in tyrosinases (phenol → *o*-quinone)[8,12] and catechol oxidase (*o*-catechol → *o*-quinone).[12−14] $Cu-O_2$ (1:1) adducts are suggested to be involved in the activities of dopamine β-hydroxylase[15,16] and amine oxidases,[17−21] and Cu_3-O_2 adducts form in multicopper oxidases (MCOs) reducing O_2 to water.[9] Low-resolution X-ray structures of O_2-adducts have been reported for copper amine oxidase,[17] laccase (an MCO)[22] and for the heme-copper active site in cytochrome *c* oxidase.[23]

Recent advances in copper−dioxygen chemistry of synthetic complexes[1−5,7] have shown that the ligand (i.e., its denticity, chelate ring size, donor type, substituents on or near N-donors) dramatically influences Cu_2-O_2 structure and reactivity. Generally, tetradentate N-donor ligands give the end-on μ-1,2-peroxo coordination,[24−27] while tridentate or bidentate N-donor ligands yield side-on μ-η^2:η^2-peroxodicopper(II) complexes, or related bis-μ-oxo-dicopper(III) species;[28−36] these normally are in rapid equilibrium.[28,32,37] Other well-characterized synthetically derived complexes possessing intact O−O bonds are known, including mono- or dicopper(II) species with a superoxo (O_2^-),[38−40] hydroperoxo (HOO^-),[41−45] or ROO^- moiety.[46−48] Several interesting μ_4-peroxo tetracopper(II) complexes have also been structurally characterized.[49,50]

In fact, the chemistry of $[(L^H)Cu^I(MeCN)]^+$ (**1**) (Figure 1; $L^H \equiv$ TMPA $\equiv$ tris(2-pyridylmethyl)amine)[51] has been quite prominent in copper−dioxygen reactivity studies. The product of low-temperature (i.e., 193 K) O_2-reaction of **1** is $[\{(L^H)Cu^{II}\}_2(O_2^{2-})]^{2+}$ (**3**) (Figure 1), whose X-ray structure (the first in Cu_2-O_2 chemistry),[24,25] spectroscopic/electronic properties,[52] and kinetics/thermodynamics[53,54] of formation

(4) Blackman, A. G.; Tolman, W. B. In *Structure & Bonding*; Meunier, B., Ed.; Springer-Verlag: Berlin: 2000; Vol. 97; pp 179−211.
(5) Suzuki, M.; Furutachi, H.; Okawa, H. *Coord. Chem. Rev.* **2000**, *200−202*, 105−129.
(6) Que, L., Jr.; Tolman, W. B. *Angew. Chem., Int. Ed.* **2002**, *41*, 1114−1137.
(7) Zhang, C. X.; Liang, H.-C.; Humphreys, K. J.; Karlin, K. D. In *Advances in Catalytic Activation of Dioxygen by Metal Complexes* (Simándi, L. I., Ed.); *Catalysis by Metal Complexes, Vol. 26* (James, B. R., van Leeuwen, P. W. N. M., Eds.); Kluwer: Dordrecht, Boston, London, 2003; Chapter 2, pp 79−121.
(8) Solomon, E. I.; Sundaram, U. M.; Machonkin, T. E. *Chem. Rev.* **1996**, *96*, 2563−2605.
(9) Solomon, E. I.; Chen, P.; Metz, M.; Lee, S.-K.; Palmer, A. E. *Angew. Chem., Int. Ed.* **2001**, *40*, 4570−4590.
(10) Magnus, K. A.; Hazes, B.; Ton-That, H.; Bonaventura, C.; Bonaventura, J.; Hol, W. G. J. *Proteins: Struct., Funct., Genet.* **1994**, *19*, 302−309.
(11) Cuff, M. E.; Miller, K. I.; van Holde, K. E.; Hendrickson, W. A. *J. Mol. Biol.* **1998**, *278*, 855−870.
(12) Decker, H.; Dillinger, R.; Tuczek, F. *Angew. Chem., Int. Ed.* **2000**, *39*, 1591−1595.
(13) Gerdemann, C.; Eicken, C.; Krebs, B. *Acc. Chem. Res.* **2002**, *35*, 183−191.
(14) Henson, M. J.; Solomon, E. I. *Chemtracts-Inorg. Chem.* **2000**, *13*, 97−102.
(15) Klinman, J. P. *Chem. Rev.* **1996**, *96*, 2541−2561.
(16) Blain, I.; Slama, P.; Giorgi, M.; Tron, T.; Reglier, M. *Rev. Mol. Biotechnol.* **2002**, *90*, 95−112.
(17) Wilmot, C. M.; Hajdu, J.; McPherson, M. J.; Knowles, P. F.; Phillips, S. E. V. *Science* **1999**, *286*, 1724−1728.
(18) Parsons, M. R.; Convery, M. A.; Wilmot, C. M.; Yadav, K. D. S.; Blakeley, V.; Corner, A. S.; Phillips, S. E. V.; McPherson, M. J.; Knowles, P. F. *Structure* **1995**, *3*, 1171−1184.
(19) Kumar, V.; Dooley, D. M.; Freeman, H. C.; Guss, J. M.; Harvey, I.; McGuirl, M. A.; Wilce, M. C. J.; Zubak, V. M. *Structure* **1996**, *4*, 943−955.
(20) Wilce, M. C. J.; Dooley, D. M.; Freeman, H. C.; Guss, J. M.; Matsunami, H.; McIntire, W. S.; Ruggiero, C. E.; Tanizawa, K.; Yamaguchi, H. *Biochemistry* **1997**, *36*, 16116−16133.
(21) Li, R.; Klinman, J. P.; Mathews, F. S. *Structure* **1998**, *6*, 293−307.
(22) Hakulinen, N.; Kiiskinen, L.-L.; Kruus, K.; Saloheimo, M.; Paananen, A.; Koivula, A.; Rouvinen, J. *Nat. Struct. Biol.* **2002**, *9*, 601−605.
(23) Yoshikawa, S.; Shinzawa-Itoh, K.; Nakashima, R.; Yaono, R.; Yamashita, E.; Inoue, N.; Yao, M.; Jei-Fei, M.; Libeu, C. P.; Mizushima, T.; Yamaguchi, H.; Tomizaki, T.; Tsukihara, T. *Science* **1998**, *280*, 1723−1729.
(24) Jacobson, R. R.; Tyeklár, Z.; Karlin, K. D.; Liu, S.; Zubieta, J. *J. Am. Chem. Soc.* **1988**, *110*, 3690−3692.
(25) Tyeklár, Z.; Jacobson, R. R.; Wei, N.; Murthy, N. N.; Zubieta, J.; Karlin, K. D. *J. Am. Chem. Soc.* **1993**, *115*, 2677−2689.
(26) Halfen, J. A.; Young, J., V. G.; Tolman, W. B. *J. Am. Chem. Soc.* **1996**, *118*, 10920−10921.
(27) Comba, P.; Hilfenhaus, P.; Karlin, K. D. *Inorg. Chem.* **1997**, *36*, 2309−2313.
(28) Halfen, J. A.; Mahapatra, S.; Wilkinson, E. C.; Kaderli, S.; Young, V. G., Jr.; Que, L., Jr.; Zuberbühler, A. D.; Tolman, W. B. *Science* **1996**, *271*, 1397−1400.
(29) Tolman, W. B. *Acc. Chem. Res.* **1997**, *30*, 227−237.
(30) Mahadevan, V.; Hou, Z.; Cole, A. P.; Root, D. E.; Lal, T. K.; Solomon, E. I.; Stack, T. D. P. *J. Am. Chem. Soc.* **1997**, *119*, 11996−11997.
(31) Mahadevan, V.; DuBois, J. L.; Hedman, B.; Hodgson, K. O.; Stack, T. D. P. *J. Am. Chem. Soc.* **1999**, *121*, 5583−5584.
(32) Mahadevan, V.; Henson, M. J.; Solomon, E. I.; Stack, T. D. P. *J. Am. Chem. Soc.* **2000**, *122*, 10249−10250.
(33) Itoh, S.; Nakao, H.; Berreau, L. M.; Kondo, T.; Komatsu, M.; Fukuzumi, S. *J. Am. Chem. Soc.* **1998**, *120*, 2890−2899.
(34) Itoh, S.; Taki, M.; Nakao, H.; Holland, P. L.; Tolman, W. B.; Que, L., Jr.; Fukuzumi, S. *Angew. Chem., Int. Ed.* **2000**, *39*, 398−400.
(35) Obias, H. V.; Lin, Y.; Murthy, N. N.; Pidcock, E.; Solomon, E. I.; Ralle, M.; Blackburn, N. J.; Neuhold, Y.-M.; Zuberbühler, A. D.; Karlin, K. D. *J. Am. Chem. Soc.* **1998**, *120*, 12960−12961.
(36) Straub, B. F.; Rominger, F.; Hofmann, P. *Chem. Commun.* **2000**, 1611−1612.
(37) Holland, P. L.; Tolman, W. B. *Coord. Chem. Rev.* **1999**, *190−192*, 855−869.
(38) Fujusawa, K.; Tanaka, M.; Moro-oka, Y.; Kitajima, N. *J. Am. Chem. Soc.* **1994**, *116*, 12079−12080.
(39) Mahroof-Tahir, M.; Karlin, K. D. *J. Am. Chem. Soc.* **1992**, *114*, 7599−7601.
(40) Chaudhuri, P.; Hess, H.; Weyhermüller, T.; Wieghardt, K. *Angew. Chem., Int. Ed.* **1999**, *38*, 1095−1098.
(41) Karlin, K. D.; Cruse, R. W.; Gultneh, Y. *J. Chem. Soc., Chem. Commun.* **1987**, 596−600.
(42) Wada, A.; Harata, M.; Hasegawa, K.; Jitsukawa, K.; Masuda, H.; Mukai, M.; Kitagawa, T.; Einaga, H. *Angew. Chem., Int. Ed.* **1998**, *37*, 798−799.
(43) Karlin, K. D.; Ghosh, P.; Cruse, R. W.; Farooq, A.; Gultneh, Y.; Jacobson, R. R.; Blackburn, N. J.; Strange, R. W.; Zubieta, J. *J. Am. Chem. Soc.* **1988**, *110*, 6769−6780.
(44) Ohta, T.; Tachiyama, T.; Yoshizawa, K.; Yamabe, T.; Uchida, T.; Kitagawa, T. *Inorg. Chem.* **2000**, *39*, 4358−4369.
(45) Mahroof-Tahir, M.; Murthy, N. N.; Karlin, K. D.; Blackburn, N. J.; Shaikh, S. N.; Zubieta, J. *Inorg. Chem.* **1992**, *31*, 3001−3003.
(46) Kitajima, N.; Fujisawa, K.; Moro-oka, Y. *Inorg. Chem.* **1990**, *29*, 357−358.
(47) Sanyal, I.; Ghosh, P.; Karlin, K. D. *Inorg. Chem.* **1995**, *34*, 3050−3056.
(48) Ghosh, P.; Tyeklár, Z.; Karlin, K. D.; Jacobson, R. R.; Zubieta, J. *J. Am. Chem. Soc.* **1987**, *109*, 6889−6891.
(49) Meyer, F.; Pritzkow, H. *Angew. Chem., Int. Ed.* **2000**, *39*, 2112−2115.
(50) Reim, J.; Werner, R.; Haase, W.; Krebs, B. *Chem. Eur. J.* **1998**, *4*, 289−298.
(51) In our previous papers, i.e., refs 2, 7, 24, 25, 52−55, 59, 74, 85, and 108, L^H is called TMPA (or tmpa); it is also more commonly referred to as TPA (or tpa).
(52) Baldwin, M. J.; Ross, P. K.; Pate, J. E.; Tyeklár, Z.; Karlin, K. D.; Solomon, E. I. *J. Am. Chem. Soc.* **1991**, *113*, 8671−8679.
(53) Karlin, K. D.; Kaderli, S.; Zuberbühler, A. D. *Acc. Chem. Res.* **1997**, *30*, 139−147.

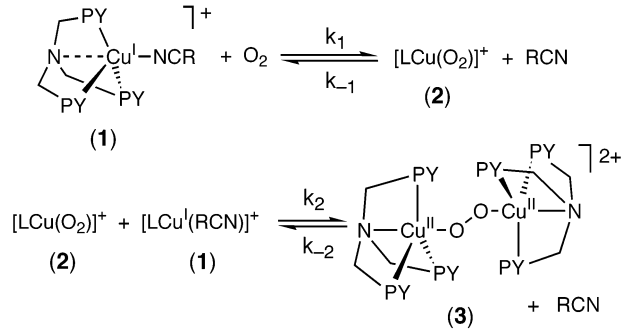

Figure 1. Previously deduced kinetic scheme for the reaction of [(L^{H})-Cu^{I}(MeCN)]$^{+}$ (**1**) with dioxygen in EtCN as solvent.

have been elucidated. Complex **3** has a bound dioxygen ligand coordinated as a μ-1,2-peroxodicopper(II) moiety, λ_{max} = 525 nm ($\epsilon \sim 10\,500$), and ν_{O-O} = 831 cm^{-1} (resonance Raman spectroscopy). A cupric superoxo intermediate [(L^{H})Cu^{II}(O$_2^{-}$)]$^{+}$ (**2**) (λ_{max} = 410 nm) forms during the reaction proceeding to **3** (Figure 1).

In the present study, we describe the use of modified L^{H} tetradentate ligands; rather than elucidate ligand structural and/or steric variations (i.e., quinolyl-for-pyridyl,[53,54] change in chelate ring size,[55] pyridyl 6-methyl substituents,[56,57] or binucleating versions[58,59]), 4-pyridyl substituents are incorporated for the purpose of investigating kinetics and thermodynamics of (L^{H})Cu^{I}/O$_2$ reaction, as influenced by *purely* electronic effects.

Ligand electronic properties have been shown to significantly influence the dioxygen affinities of synthetic iron(II) and cobalt(II) dioxygen carriers.[60−63] Using a series of linear polyamine ligands, Martell and co-workers have reported a linear correlation between the dioxygen binding constants and the logarithms of the total basicity of the ligand donor group.[64,65] With a series of cobalt(II) Schiff base complexes, it has also been shown that log(K_{O2}) for the formation of the 1:1 Co−O$_2$ complex is linearly related to the Co^{III}/Co^{II} reduction potentials.[66] Similar results have been found for the heme systems. For hemes, Traylor et al.[67,68] reported that

Chart 1

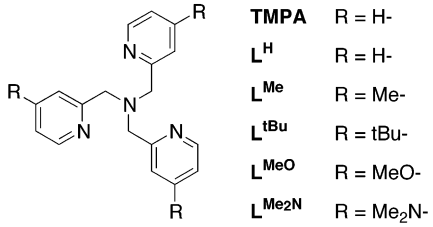

[(L^{R})Cu^{I}(MeCN)]$^{+}$ (**1^{R}**)
[(L^{R})Cu^{II}(O$_2^{-}$)]$^{+}$ (**2^{R}**)
[{(L^{R})Cu^{II}}$_2$(O$_2^{2-}$)]$^{2+}$ (**3^{R}**)

electron-withdrawing groups on the porphyrin ring periphery diminish the dioxygen affinity by increasing the dioxygen dissociation rate constant. Equally, increasing donor strength of the axial base significantly increases the dioxygen binding affinity to ferrous porphyrin complexes.[69−73]

In contrast to Fe(II) and Co(II) systems, no detailed studies on how ligand electronic effects influence the O$_2$-reactions with copper(I) complexes have been reported. Here we use the well-defined L^{H} (≡TMPA) system as a starting point to systematically vary the ligand electronic properties; a 4-pyridyl substituent should exert no or minimal steric effects upon the resulting chemistry (Chart 1). The present stopped-flow kinetic investigations show that there can be significant ligand (L^{R}) electronic and solvent effects on the oxygenation reactions of the resulting copper(I) complexes. Ligand electronic effects are also manifested in the electrochemistry and ν(CO) of [LCu^{I}−CO]$^{+}$ complexes. The results are significant in terms of developing a fundamental understanding of copper(I)/dioxygen chemistry, which may contribute to bioinorganic problems as well as to chemical applications.

Results and Discussion

Ligand Syntheses. Electronic effects for (ligand)Cu^{I}/O$_2$ reactivity studies were carried out by utilizing tripodal tetradentate L^{R} (see Introduction) ligands.

The ligand L^{Me} was synthesized by following a literature-based procedure,[74] while L^{tBu}, L^{MeO}, and L^{Me_2N} were prepared in a similar manner as shown in Scheme 1. Further details are given in the Experimental Section. As can be seen, the substituents chosen for these studies range from Me to Me$_2$N, which are electron-donating groups. Synthetic difficulties

(54) Karlin, K. D.; Wei, N.; Jung, B.; Kaderli, S.; Niklaus, P.; Zuberbühler, A. D. *J. Am. Chem. Soc.* **1993**, *115*, 9506−9514.
(55) Schatz, M.; Becker, M.; Thaler, F.; Hampel, F.; Schindler, S.; Jacobson, R. R.; Tyeklár, Z.; Murthy, N. N.; Ghosh, P.; Chen, Q.; Zubieta, J.; Karlin, K. D. *Inorg. Chem.* **2001**, *40*, 2312−2322.
(56) Hayashi, H.; Fujinami, S.; Nagatomo, S.; Ogo, S.; Suzuki, M.; Uehara, A.; Watanabe, Y.; Kitagawa, T. *J. Am. Chem. Soc.* **2000**, *122*, 2124−2125.
(57) Hayashi, H.; Uozumi, K.; Fujinami, S.; Nagatomo, S.; Shiren, K.; Furutachi, H.; Suzuki, M.; Uehara, A.; Kitagawa, T. *Chem. Lett.* **2002**, 416−417.
(58) Lee, D.-H.; Wei, N.; Murthy, N. N.; Tyeklár, Z.; Karlin, K. D.; Kaderli, S.; Jung, B.; Zuberbühler, A. D. *J. Am. Chem. Soc.* **1995**, *117*, 12498−12513.
(59) Karlin, K. D.; Lee, D.-H.; Kaderli, S.; Zuberbühler, A. D. *Chem. Commun.* **1997**, 475−476.
(60) Jones, R. D.; Summerville, D. A.; Basolo, F. *Chem. Rev.* **1979**, *79*, 139−179.
(61) Niederhoffer, E. C.; Timmons, J. H.; Martell, A. E. *Chem. Rev.* **1984**, *84*, 137.
(62) Warburton, P. R.; Busch, D. H. *Perspect. Bioinorg. Chem.* **1993**, *2*, 1−79.
(63) *Oxygen Complexes and Oxygen Activation by Transition Metals*; Martell, A. E., Sawyer, D. T., Ed.; Plenum: New York, 1988.
(64) McLendon, G. L.; Martell, A. E. *Chem. Commun.* **1975**, 223.
(65) Harris, W. R.; Timmons, J. H.; Martell, A. E. *J. Coord. Chem.* **1979**, *8*, 251.
(66) Carter, M. J.; Rillema, D. P.; Basolo, F. *J. Am. Chem. Soc.* **1974**, *96*, 392−400.
(67) Traylor, T. G.; White, D. K.; Campbell, D. H.; Berzinis, A. P. *J. Am. Chem. Soc.* **1981**, *103*, 4932−4936.
(68) Traylor, T. G.; Traylor, P. S. In *Active Oxygen: Active Oxygen in Biochemistry*; Valentine, J. S., Foote, C. S., Greenberg, A., Liebman, J. F., Eds.; Chapman & Hall: New York, 1995; pp 84−187.
(69) Momenteau, M.; Loock, B.; Lavaletter, D.; Tetreau, C.; Mispelter, J. *Chem. Commun.* **1983**, 962−964.
(70) Collman, J. P.; Brauman, J. I.; Doxsee, K. M.; Sessler, J. L.; Morris, R. M.; Gibson, O. H. *Inorg. Chem.* **1983**, *22*, 1427−1432.
(71) Traylor, T. G.; Traylor, P. S. *Annu. Rev. Biophys. Bioeng.* **1982**, *11*, 105−127.
(72) Brinigar, W. S.; Chang, C. K.; Geibel, J.; Traylor, T. G. *J. Am. Chem. Soc.* **1974**, *96*, 5597−5599.
(73) Momenteau, M.; Reed, C. A. *Chem. Rev.* **1994**, *94*, 659−698.
(74) Nanthakumar, A.; Fox, S.; Murthy, N. N.; Karlin, K. D. *J. Am. Chem. Soc.* **1997**, *119*, 3898−3906.

Scheme 1

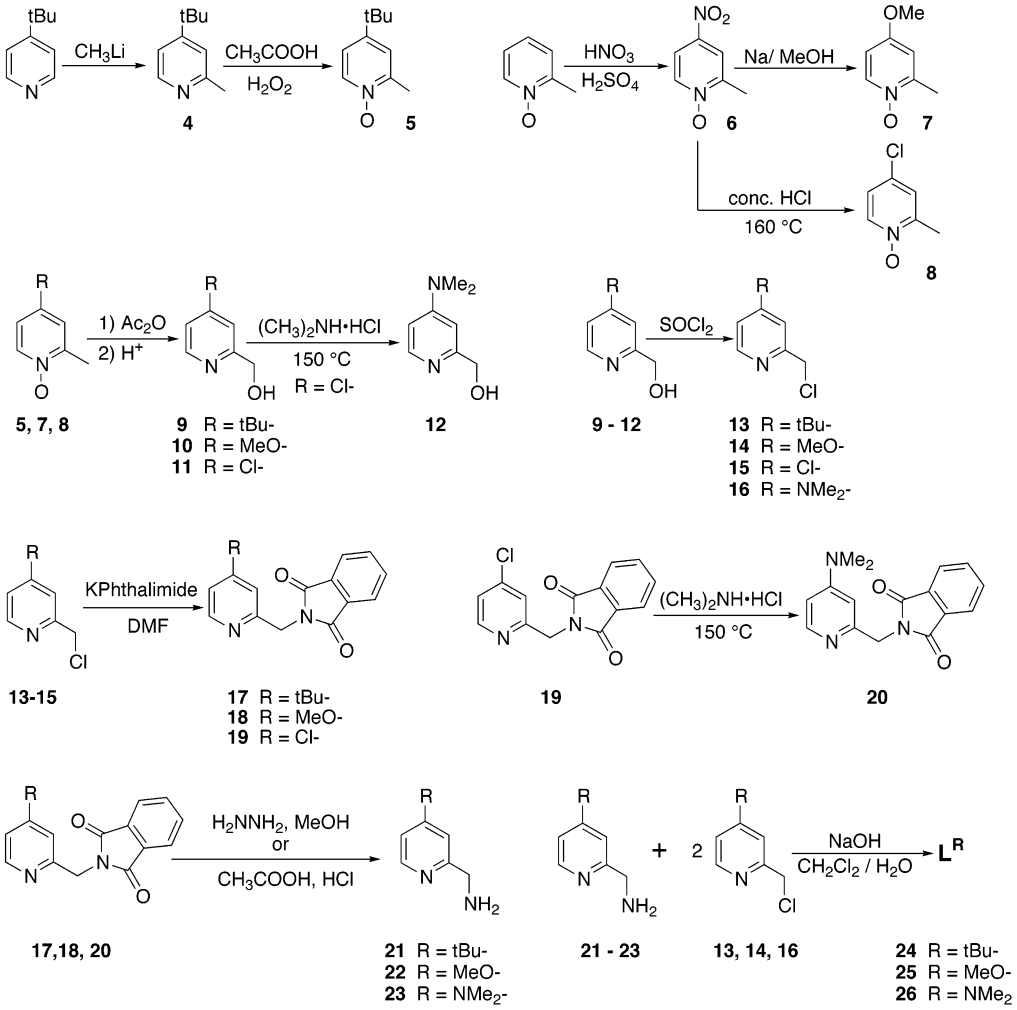

encountered were the cause for not including any examples of electron-withdrawing groups, although this would have been of interest.[75] A 4-NO_2 group was used as a precursor for introducing desired R groups onto the 4-pyridyl positions; however, we found that it was labile and the 4-NO_2 group did not survive the later steps required for ligand preparation.

Syntheses of Copper(I) Complexes. Copper(I) complexes $[(L^R)Cu^I(MeCN)]ClO_4$ used for the kinetic studies in EtCN and acetone as solvents were synthesized by mixing 1 equiv each of ligand L^R and $[Cu(MeCN)_4]ClO_4$ under an Ar atmosphere in acetonitrile (MeCN) solution. Due to the low solubilities of these complexes in THF, the corresponding copper(I) complexes with $BArF^-$ (tetrakis(3,5-bis-trifluoromethylphenyl)borate) as counteranion were prepared by metathesis reactions between $[(L^R)Cu^I(MeCN)](ClO_4)$ and NaBArF (see Experimental Section). Interestingly, the isolated Cu(I)-complex with L^{Me_2N} ligand readily adopts a 4-coordinate formulation $[(L^{Me_2N})Cu^I]^+$ without incorporating MeCN as its fifth ligand[76] even when prepared and isolated in MeCN as solvent. This is in contrast to the analogous complexes with L^R (R = H, Me, tBu, and MeO) which prefer pentacoordination geometry when prepared in MeCN. This may possibly be rationalized by ligand electronic effects, where a more electron-rich ligand (L^{Me_2N}) can provide more electron density to the copper(I) center which then disfavors the coordination of an additional RCN ligand.[77] The coordinated nitrile ligand in these complexes with $BArF^-$ as anion can in general be removed by recrystallization from a noncoordinating solvent such as diethyl ether.

Electrochemistry. The electrochemical behavior of the copper(I) complexes was measured by cyclic voltammetry (CV) under Ar in MeCN solution. The data are given in Table 1. The copper(I) complexes $[(L^R)Cu^I(MeCN)]^+$ display single quasireversible redox behavior with i_{pa}/i_{pc} varying from 0.91 to 1.05. Peak separations were all less than 110 mV at a scan rate of 100 mV/s. The Cu^{II}/Cu^I reduction potentials measured for the copper(I) complexes are reported relative to the ferrocene−ferrocenium couple which was used as an external reference.

(75) It should be noted that in 4-pyridyl substituted MePY2 tridentate ligands, {MePY2 ≡ *N*-(methyl)-*N*,*N*-bis(2-pyridylethylamine)}, we found that the Cl-substituted ligand copper(I) complex did not even react with O_2. Zhang, C. X.; Liang, H.-C.; Kim, E.-i.; Shearer, J.; Helton, M. E.; Kim, E.; Kaderli, S.; Incarvito, C. D.; Zuberbühler, A. D.; Rheingold, A. L.; Karlin, K. D. *J. Am. Chem. Soc.* **2003**, *125*, 634−635.

(76) Lim, B. S.; Holm, R. H. *Inorg. Chem.* **1998**, *37*, 4898−4908.

(77) Storhoff, B. N.; Lewis, H. C., Jr. *Coord. Chem. Rev.* **1977**, *23*, 1−29.

Table 1. Cyclic Voltammetry Data for Cu(I) Complexes in CH_3CN[a]

complex	$E_{1/2}$ (V)	ΔE_p (mV)	i_{pa}/i_{pc}
[(L^{H})Cu^{I}(MeCN)]$^{+}$ (**1^{H}**)	−0.40	79	0.91
[(L^{t}Bu)Cu^{I}(MeCN)]$^{+}$ (**1^{tBu}**)	−0.46	84	1.01
[(L^{MeO})Cu^{I}(MeCN)]$^{+}$ (**1^{MeO}**)	−0.49	76	1.05
[(L^{Me_2N})Cu^{I}]$^{+}$ (**1^{Me_2N}**)	−0.70	106	0.98

[a] Potentials are versus Fc/Fc^{+}, measured under the same elctrochemical cell conditions.

Table 2. Carbonyl Stretching Frequencies for [(L^{R})Cu^{I}(CO)]$^{+}$ Complexes

	1^{H}	**1^{tBu}**	**1^{MeO}**	**1^{Me_2N}**
ν(CO) (cm^{-1})	2092	2089	2087	2079

The data shown in Table 1 reveal that, with 4-substituted pyridyl ligands L^{R}, the $E_{1/2}$ values for the (L^{R})Cu^{II}/(L^{R})Cu^{I} redox couple become more negative compared to that for the complex with the parent ligand L^{H}, resulting in more thermodynamically stable Cu(II) complexes. In other words, as the R group becomes more electron-donating (i.e., R = OMe vs tBu vs H), more negative values for the Cu^{II}/Cu^{I} reduction potentials are observed making it easier to oxidize Cu(I) to Cu(II). The observed ligand effect upon $E_{1/2}$ correlates to the difference in ligand basicity. The pK_a values for pyridine, 4-Me-pyridine (similar to 4-tBu-pyridine), 4-MeO-pyridine, and 4-Me$_2$N-pyridine are 5.21, 6.03, 6.58, and 9.70, respectively.[78,79] We previously observed that the difference in electrochemical behavior of copper(I) complexes with pyridyl and/or quinolyl ligands did relate to variations in their O_2 reactivity. However, in those cases, steric effects probably dominate.[54]

CO Stretching Frequencies for the Carbonyl Complexes. The carbonyl complexes [(L^{R})Cu^{I}(CO)]$^{+}$ were obtained by bubbling the MeCN solutions of the corresponding copper(I) species [(L^{R})Cu^{I}(MeCN)]ClO$_4$ (**1^{R}**) with CO, and their in situ IR spectra indicated the presence of CO stretching bands in the range 2079−2092 cm^{-1}. The Cu/CO 1:1 stoichiometry is indicated by our previous studies with [(L^{H})Cu^{I}(CO)]$^{+}$,[25] by the single observed IR-band and the known tendency for Cu(I) complexes with N_3 or N_4 ligands.[80] The carbonyl stretching frequencies generally decrease with increasing electron density on the ligand due to the π-backbonding interaction effected through the metal center that weakens the CO bond. Here, the observed ν(CO) shift (Table 2) is consistent with this picture, where the most electron-donating ligand **L^{Me_2N}** exhibits the lowest ν(CO) frequency.

The CO adducts of copper-containing proteins with tris(imidazole) coordination core for the copper centers (e.g., in hemocyanins, amine oxidases, peptidylglycine monooxygenase, and cytochrome *c* oxidase) have been reported to exhibit ν(CO) in the range 2043−2063 cm^{-1}.[80] However, in synthetic complexes, comparable CO stretching frequencies (2059−2067 cm^{-1}) have been observed only with non-chelating imidazole ligands or anionic tris(pyrazolyl)borate ligands. The copper CO complexes with neutral ligands in general exhibit stronger CO bonding with higher ν(CO) frequencies in the range 2080−2102 cm^{-1}.[80] Ligand constraints, which affect the geometry around the copper center for CO binding, and electronic properties of the donor groups[81] contribute to the differences in ν(CO) values observed for the CO adducts of the proteins and model complexes.

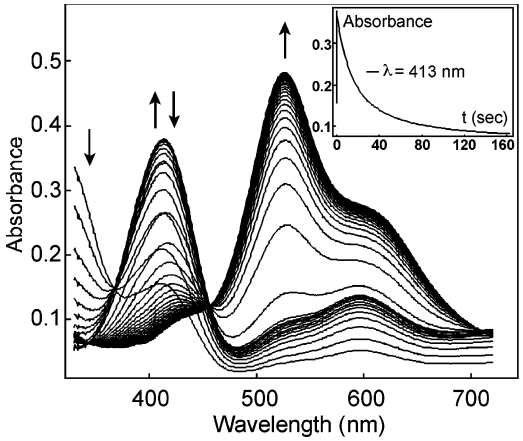

Figure 2. Time-dependent UV−vis spectra for the oxygenation of [(L^{MeO})Cu^{I}(RCN)]$^{+}$ (**1^{MeO}**) at 179 K. Inset: absorbance vs time at 413 nm.

Kinetics of Oxygenation Reactions. The kinetic scheme[53,54] of the reaction of [(L^{H})Cu(EtCN)](ClO$_4$) (**1^{H}**) with dioxygen in EtCN is outlined in Figure 1 (Introduction). However, when the chemistry was carried out with the parent complex in acetone, the stopped-flow kinetics revealed that a superoxocopper(II) species [(L^{H})Cu^{II}(O$_2^{-}$)]$^{+}$ (**2^{H}**) with λ_{max} = 420 nm formed within the stopped-flow mixing time (even at 183 K), and the peroxo complex [{(L^{H})Cu^{II}}$_2$(O$_2^{2-}$)]$^{2+}$ (**3^{H}**) exhibited reasonable room temperature (rt) stability.[59,82] This shows that solvent medium is very important in LCu^{I}/O_2 reactivity. To further elucidate the fundamental aspects of this copper−dioxygen interaction, we carried out the present extended kinetic study on the oxygenation reactions of mononuclear copper(I) complexes [(L^{R})Cu^{I}(MeCN)]$^{+}$ with 4-pyridyl substituted ligand analogues L^{R} (R = Me, tBu, MeO) (Chart 1) in different media (EtCN, THF, and acetone).

1. Oxygenation Reactions of Copper(I) Complexes [(L^{R})Cu(MeCN)](ClO$_4$) in EtCN. The interaction of [(L^{R})Cu^{I}(RCN)]$^{+}$ (R = Me or Et) with dioxygen in EtCN follows the same basic mechanism which has been found in the analogous reaction of [(L^{H})Cu(RCN)]$^{+}$ (Figure 1). At low temperature, [(L^{R})Cu(RCN)]$^{+}$ reacts in a reversible fashion with a dioxygen molecule to form a 1:1 Cu−O_2 species which further reacts reversibly with [(L^{R})Cu(RCN)]$^{+}$ ion to form the dinuclear 2:1 Cu_2O_2 adduct. Figure 2 shows the UV−vis behavior when, for example, [(L^{MeO})Cu(RCN)]$^{+}$ (**1^{MeO}**) reacts with excess O_2 at 179 K. Upon mixing of solutions of O_2 and **1^{MeO}**, there is a fast formation of species [(L^{MeO})Cu^{II}(O$_2^{-}$)]$^{+}$ (**2^{MeO}**) with λ_{max} at 413 and 598

(78) Schofield, K. In *Hetero-aromatic Nitrogen Compounds*; Butterworths: London, 1967; p 146.
(79) Höfle, G.; Steglich, W.; Vorbrüggen, H. *Angew. Chem., Int. Ed. Engl.* **1978**, *17*, 569.
(80) Rondelez, Y.; Sénèque, O.; Rager, M.-N.; Duprat, A. F.; Reinaud, O. *Chem. Eur. J.* **2000**, *6*, 4218−4226.
(81) Hirsch, J.; George, S. D.; Solomon, E. I.; Hedman, B.; Hodgson, K. O.; Burstyn, J. N. *Inorg. Chem.* **2001**, *40*, 2439−2441.
(82) Detailed numerical analysis was not possible for this "parent" system (R = H) because of recurring deviations from ideal behavior expected for reasonably simple mechanistic schemes.

Table 3. Kinetic Parameters for O_2-Interaction with $[(L^R)Cu^I(RCN)]^+$ (in EtCN) and $[(L^R)Cu^I]^+$ (in THF)[a]

	EtCN					THF[d] R= H
parameter	R = H[b]	R = H[c]	R = Me	R = tBu	R = MeO	
			k_1 (M^{-1} s^{-1})			
$\Delta H^{\ddagger}$ [e]	32 ± 4	31.6 ± 0.5	29.1 ± 0.5	31.8 ± 0.4	30.5 ± 0.6	
$\Delta S^{\ddagger}$ [f]	14 ± 18	10 ± 3	0 ± 3	19 ± 2	8 ± 3	
183 K	(1.8 ± 0.1) × 10^4	(1.18 ± 0.01) × 10^4	(1.95 ± 0.02) × 10^4	(3.11 ± 0.02) × 10^4	(1.93 ± 0.04) × 10^4	≥2 × 10^6
223 K	(9 ± 4) × 10^5	(5.0 ± 0.3) × 10^5	(7.3 ± 0.4) × 10^5	(1.61 ± 0.08) × 10^6	(8.5 ± 0.5) × 10^5	
298 K	8 × 10^7	(5.8 ± 0.8) × 10^7	(5.0 ± 0.7) × 10^7	(1.6 ± 0.2) × 10^8	(7 ± 1) × 10^7	
			k_{-1} (s^{-1})			
$\Delta H^{\ddagger}$	66 ± 4	61.5 ± 0.5	57.8 ± 0.6	59.4 ± 0.5	62.2 ± 0.7	
$\Delta S^{\ddagger}$	137 ± 18	118 ± 3	90 ± 3	107 ± 3	100 ± 3	
183 K	8 ± 1	(1.59 ± 0.01) × 10	5.57 ± 0.08	(1.63 ± 0.02) × 10^1	1.11 ± 0.06	
223 K	(3 ± 1) × 10^4	(2.7 ± 0.2) × 10^4	(6.2 ± 0.4) × 10^3	(2.2 ± 0.1) × 10^4	(2.1 ± 0.1) × 10^3	
298 K	2 × 10^8	(1.5 ± 0.2) × 10^8	(2.1 ± 0.3) × 10^7	(9 ± 1) × 10^7	(1.3 ± 0.2) × 10^7	
			k_2 ($M^{-1}s^{-1}$)			
$\Delta H^{\ddagger}$	14 ± 1	22.6 ± 0.1	19.3 ± 0.2	16.67 ± 0.08	20.59 ± 0.06	17.5 ± 0.1
$\Delta S^{\ddagger}$	−78 ± 2	−38.6 ± 0.6	−51.6 ± 0.8	−61.4 ± 0.4	−46.7 ± 0.3	−50 ± 1
183 K	(3.2 ± 0.2) × 10^4	(1.34 ± 0.02) × 10^4	(2.45 ± 0.05) × 10^4	(4.10 ± 0.04) × 10^4	(1.85 ± 0.01) × 10^4	(1.0 ± 0.2) × 10^5
223 K	(2.48 ± 0.02) × 10^5	(2.33 ± 0.02) × 10^5	(2.89 ± 0.04) × 10^5	(3.57 ± 0.02) × 10^5	(2.56 ± 0.01) × 10^5	(9.53 ± 0.08) × 10^5
298 K	(1.8 ± 0.1) × 10^6	(6.7 ± 0.2) × 10^6	(5.3 ± 0.2) × 10^6	(4.58 ± 0.06) × 10^6	(5.58 ± 0.06) × 10^6	(1.36 ± 0.03) × 10^7
			k_{-2} (s^{-1})			
$\Delta H^{\ddagger}$	61 ± 3	69.8 ± 0.6	67.4 ± 0.5	66.4 ± 0.6	69 ± 1	70 ± 4
$\Delta S^{\ddagger}$	19 ± 10	51 ± 3	40 ± 2	38 ± 3	40 ± 5	32 ± 14
183 K	(1.5 ± 0.8) × 10^{-4}	(2.0 ± 0.2) × 10^{-5}	(2.6 ± 0.2) × 10^{-5}	(4.1 ± 0.5) × 10^{-5}	(8 ± 2) × 10^{-6}	2 × 10^{-6}
223 K	(2.9 ± 0.4) × 10^{-1}	(9.1 ± 0.4) × 10^{-2}	(8.9 ± 0.3) × 10^{-2}	(1.26 ± 0.06) × 10^{-1}	(3.4 ± 0.4) × 10^{-2}	(9 ± 4) × 10^{-3}
298 K	(1.2 ± 0.3) × 10^3	(1.6 ± 0.1) × 10^3	(1.12 ± 0.07) × 10^3	(1.38 ± 0.09) × 10^3	(5.5 ± 0.4) × 10^2	(1.6 ± 0.4) × 10^2
			k_{on} (=$K_1 \times k_2$) (M^{-2} s^{-1})			
$\Delta H^{\ddagger}$	−20 ± 2	−7.3 ± 0.2	−9.5 ± 0.3	−10.9 ± 0.2	−11.2 ± 0.4	−24 ± 2
$\Delta S^{\ddagger}$	−201 ± 5	−147 ± 1	−141 ± 1	−150 ± 1	−139 ± 2	−162 ± 9
183 K	(6.2 ± 0.5) × 10^7	(9.9 ± 0.2) × 10^6	(8.6 ± 0.2) × 10^7	(7.8 ± 0.1) × 10^7	(3.2 ± 0.2) × 10^8	(7 ± 3) × 10^{10}
223 K	(6.4 ± 0.4) × 10^6	(5.1 ± 0.1) × 10^6	(3.40 ± 0.08) × 10^7	(2.62 ± 0.05) × 10^7	(1.04 ± 0.02) × 10^8	(5.3 ± 0.5) × 10^9
298 K	(6 ± 1) × 10^5	(2.6 ± 0.1) × 10^6	(1.24 ± 0.07) × 10^7	(7.9 ± 0.4) × 10^6	(3.0 ± 0.2) × 10^7	(2.9 ± 0.7) × 10^8

[a] Constants k_1 and k_2 are determined experimentally, while k_{-1} (=k_1/K_1) and k_{on} (=$k_2 \times K_1$) are calculated. [b] Previously published data. [c] Recent data collected on a new instrument with faster sampling time. While activation parameters show some differences between old and new measurements, actual rate constants measured, i.e., those with low associated errors, are rather close. [d] No RCN involved in this solvent. [e] Units for $\Delta H^{\ddagger}$ values: kJ mol^{-1}. [f] Units for $\Delta S^{\ddagger}$ values: J K^{-1} mol^{-1}.

nm; this quickly decays (~20 s) and is transformed into $[\{(L^{MeO})Cu^{II}\}_2(O_2^{2-})]^{2+}$ (**3^{MeO}**) with 525 and 595 nm absorptions. The inset of Figure 2 shows the absorbance versus time trace at 413 nm. The formation of $[(L^{MeO})Cu^{II}(O_2^{-})]^+$ (**2^{MeO}**) can only be followed below 203 K because at higher temperature it occurs faster than the stopped-flow instrumental limit (1.3 ms). Above 233 K, the formation of $[\{(L^{MeO})Cu^{II}\}_2(O_2^{2-})]^{2+}$ (**3^{MeO}**) is incomplete, and its irreversible decay to secondary products becomes significant. The variable-temperature stopped-flow data of the oxygenation reactions of $[(L^R)Cu^I(RCN)]^+$ were analyzed by global analysis in the eigenvector space,[54] and the kinetic and thermodynamic parameters deduced are listed in Tables 3 and 4.[83] Unfortunately, quantitative data for the oxygenation reaction of **1^{Me_2N}** cannot be included; its low solubility in EtCN at reduced temperatures (even with $BArF^-$ as counteranion) prevented accurate concentration measurements and full kinetic analysis. However, qualitative observations will be discussed in the following sections.

(a) Formation and Dissociation of the 1:1 Adduct $[(L^R)Cu^{II}(O_2^{-})]^+$ (2^R). As mentioned in the Introduction, $Cu-O_2$ (1:1) adducts are of interest since they are the primary products of the oxygenation reactions of Cu(I)-complexes. With a sterically hindered tridentate ligand, Kitajima and co-workers structurally characterized a side-on superoxocopper(II) complex, $Cu^{II}(O_2^{-})[HB(3\text{-}tBu\text{-}5\text{-}iPrPz)_3]$.[38] However, terminal end-on coordination is well-known for oxy-hemoglobin or oxy-myoglobin and Schiff base cobalt(III)−superoxo complexes.[61,84] No definitive structural information for the 1:1 $Cu-O_2$ adduct $[(L^R)Cu^{II}(O_2^{-})]^+$ (**2^R**) described here is available, but it is suggested to have an end-on coordination, following arguments previously published.[53,85]

As shown in Table 3, the rate constants for formation of $[(L^R)Cu^{II}(O_2^{-})]^+$ (**2^R**) (k_1) fall into a small range between 1.18×10^4 and 3.11×10^4 M^{-1} s^{-1} at 183 K with ligand L^R having different substituent groups (R = H, Me, tBu, MeO); i.e., the dioxygen association rates are hardly affected by these variations in ligand electronic environment. The O_2-binding processes are accompanied by significant activation enthalpies (29.1−31.8 kJ mol^{-1}) and small positive activation entropies (0−19 J K^{-1} mol^{-1}). The insensitivity of the O_2-binding rate constant (k_1) toward variations of substituents in L^R in R groups may be rationalized by the importance of the accompanying dissociation of a coordinated EtCN from the Cu(I)-complex during the dioxygen binding process leading to **2^R**. The same phenomenon has

(83) For Eyring and/or van't Hoff plots related to data summarized in tables on kinetic and thermodynamic parameters, see Supporting Information.

(84) Bakac, A. *Prog. Inorg. Chem.* **1995**, *43*, 267−351.

(85) Wei, N.; Murthy, N. N.; Chen, Q.; Zubieta, J.; Karlin, K. D. *Inorg. Chem.* **1994**, *33*, 1953−1965.

Table 4. Thermodynamic Parameters for O_2-Interaction with $[(L^R)Cu^I(RCN)]^+$ (in EtCN) and $[(L^R)Cu^I]^+$ (in THF)[a]

parameter	EtCN					THF[d]
	R = H[b]	R = H[c]	R= Me	R= t-Bu	R= MeO	R = H
			K_1 (M^{-1})			
$\Delta H°$ [e]	−34 ± 1	−29.8 ± 0.2	−28.8 ± 0.2	−27.6 ± 0.2	−31.8 ± 0.4	−41 ± 2
$\Delta S°$ [f]	−123 ± 4	−108 ± 1	−90 ± 1	−88 ± 1	−93 ± 2	−112 ± 9
183 K	(1.9 ± 0.1) × 10^3	(7.42 ± 0.04) × 10^2	(3.50 ± 0.04) × 10^3	(1.91 ± 0.02) × 10^3	(1.73 ± 0.08) × 10^4	(7 ± 3) × 10^5
223 K	(2.7 ± 0.2) × 10^1	(2.20 ± 0.04) × 10^1	(1.18 ± 0.02) × 10^2	(7.4 ± 0.1) × 10^1	(4.09 ± 0.06) × 10^2	(5.5 ± 0.5) × 10^3
298 K	(3.4 ± 0.8) × 10^{-1}	(3.8 ± 0.2) × 10^{-1}	2.4 ± 0.1	1.73 ± 0.08	5.5 ± 0.3	(2.1 ± 0.5) × 10^1
			K_2 (M^{-1})			
$\Delta H°$	−47 ± 3	−47.2 ± 0.6	−48.1 ± 0.4	−49.7 ± 0.6	−49 ± 1	−53 ± 4
$\Delta S°$	−97 ± 10	−89 ± 2	−91 ± 2	−99 ± 3	−87 ± 5	−82 ± 14
183 K	(2.2 ± 0.7) × 10^8	(6.7 ± 0.7) × 10^8	(9.4 ± 0.6) × 10^8	(1.0 ± 0.1) × 10^9	(2.4 ± 0.7) × 10^9	5 × 10^{10}
223 K	(8.6 ± 1.2) × 10^5	(2.6 ± 0.1) × 10^6	(3.24 ± 0.09) × 10^6	(2.8 ± 0.1) × 10^6	(7.6 ± 0.9) × 10^6	(1.1 ± 0.5) × 10^8
298 K	(1.5 ± 0.4) × 10^3	(4.2 ± 0.3) × 10^3	(4.7 ± 0.3) × 10^3	(3.3 ± 0.2) × 10^3	(1.02 ± 0.08) × 10^4	(9 ± 2) × 10^4
			$\beta = K_1K_2$ (M^{-2})			
$\Delta H°$	−81 ± 3	−77.1 ± 0.6	−76.9 ± 0.4	−77.3 ± 0.6	−81 ± 1	−94 ± 3
$\Delta S°$	−220 ± 11	−197 ± 2	−181 ± 2	−188 ± 2	−179 ± 4	−194 ± 11
183 K	(4.3 ± 1.5) × 10^{11}	(5.0 ± 0.5) × 10^{11}	(3.3 ± 0.2) × 10^{12}	(1.9 ± 0.2) × 10^{12}	(4 ± 1) × 10^{13}	4 × 10^{16}
223 K	(2.3 ± 0.4) × 10^7	(5.6 ± 0.2) × 10^7	(3.81 ± 0.09) × 10^8	(2.08 ± 0.08) × 10^8	(3.1 ± 0.4) × 10^9	(6 ± 3) × 10^{11}
298 K	(5 ± 1) × 10^2	(1.6 ± 0.1) × 10^3	(1.11 ± 0.04) × 10^4	(5.7 ± 0.3) × 10^3	(5.6 ± 0.3) × 10^4	(1.9 ± 0.1) × 10^6

[a] Constants K_1 and β ($=K_1K_2$) are determined experimentally, while K_2 ($=\beta/K_1$) is calculated. [b] Previously published data. [c] Recent data collected on a new instrument with faster sampling time. See footnote to Table 3. [d] No RCN involved in this solvent. [e] Units for $\Delta H°$ values: kJ mol^{-1}. [f] Units for $\Delta S°$ values: J K^{-1} mol^{-1}.

been observed in the aqueous oxygenation reactions of some six-coordinate cobalt(II) complexes[62,86] with very similar rate constants (k_1) for dioxygen binding to form the 1:1 Co−O_2 adducts. In addition, relatively high activation enthalpies along with positive activation entropies were found, indicative of a dissociative process (ligand/solvent dissociation is the rate-determining step). In contrast, when five-coordinate cobalt(II) complexes possessing a vacant coordination site were used in more recent O_2-binding studies, much smaller activation enthalpies (5−15 kJ mol^{-1}) and negative activation entropies were observed.[87,88]

Large activation enthalpies along with positive activation entropies are associated with the dissociation (k_{-1}) of O_2 from Cu−O_2 adducts $[(L^R)Cu^{II}(O_2^-)]^+$ (**2**). The rate constants k_{-1} (Table 3) reveal a small but significant ligand effect (1 order of magnitude decrease from $\mathbf{2^H}$ to $\mathbf{2^{MeO}}$), which thus translates into a similarly small effect (i.e., factor of ∼10) in the O_2^- binding ability (K_1, Table 4). As the R group becomes more electron-donating, the rate constant k_{-1} decreases and K_1 increases, consistent with oxygenation being accompanied by electron transfer from copper(I) to O_2 (giving superoxide anion).

(b) Formation and Dissociation of the 2:1 Adduct $[\{(L^R)Cu^{II}\}_2(O_2^{2-})]^{2+}$ ($\mathbf{3^R}$). As shown in Table 3, the association rate constants k_2 are similar for $\mathbf{3^H}$, $\mathbf{3^{Me}}$, $\mathbf{3^{tBu}}$, and $\mathbf{3^{MeO}}$. This again suggests the importance of EtCN competition in these oxygenation reactions. The activation enthalpies for k_{-2} pertaining to Cu−O bond splitting are also very similar among all Cu_2O_2 adducts. Interestingly, these activation enthalpies match the values observed for the related process k_{-1}. This may reflect similar terminal coordination for superoxocopper(II) ($\mathbf{2^R}$) and the structurally characterized peroxodicopper(II) ($\mathbf{3^R}$) species. Nevertheless, actual rate constants k_{-2} are 4−5 orders of magnitude smaller than corresponding values of k_{-1} due to significantly less favorable activation entropies. This may reflect differing influences of solvent on the Cu−O−O ($\mathbf{2^R}$) versus Cu−O−O−Cu ($\mathbf{3^R}$) copper−oxygen cleavage and/or the fact that this dissociation process for $\mathbf{2^R}$ (k_{-1}) involves the release of a dioxygen molecule.

The overall reaction to form the peroxodicopper(II) species $[\{(L^R)Cu^{II}\}_2(O_2^{2-})]^{2+}$ (**3**) is accompanied by strongly negative reaction enthalpies, which indicate strong complex formation at low temperature, along with the usual compensating large negative entropies. The thermodynamic stability for the 2:1 adduct shows relatively small differences with $\Delta H°$ in the range −77 to −81 kJ mol^{-1}. Yet, we note that the equilibrium constant for the formation of $\mathbf{3^R}$ ($\beta = K_1K_2$) increases on going from the L^H to $L^{Me,tBu}$ to L^{MeO} complex (Table 4), by a total of 2 orders of magnitude.

(c) Observations for the Oxygenation of $\mathbf{1^{Me_2N}}$. The low solubility of $[(L^{Me_2N})Cu^I(EtCN)]^+$ ($\mathbf{1^{Me_2N}}$) in EtCN leads to low reproducibility of data, and no complete kinetic analysis could be obtained. However, qualitative observations showed a remarkably different UV−vis behavior for the oxygenation reaction of complex $\mathbf{1^{Me_2N}}$ (Figure S3)[89] compared to those of the other Cu(I) complexes $\mathbf{1^R}$. The formation of the superoxocopper(II) species $[(L^{Me_2N})Cu^{II}(O_2^-)]^+$ ($\mathbf{2^{Me_2N}}$) is complete within the mixing time of the stopped-flow instrument (1.3 ms), and very little if any Cu(I)-complex $\mathbf{1^{Me_2N}}$ is present, as indicated by the lack of a 340 nm absorption. The transformation of the superoxo species into the peroxo species $[\{(L^{Me_2N})Cu^{II}\}_2(O_2^{2-})]^{2+}$ ($\mathbf{3^{Me_2N}}$) is exceedingly slow at low temperature but increases dramatically with increasing temperature (Figure S3).[89] The slower formation of the peroxo species $\mathbf{3^{Me_2N}}$ does not represent a

(86) Fallab, S.; Mitchell, P. R. *Adv. Inorg. Bioinorg. Mech.* **1984**, *3*, 311−377.
(87) Rybak-Akimova, E. V.; Otto, W.; Deardorf, P.; Roesner, R.; Busch, D. H. *Inorg. Chem.* **1997**, *36*, 2746.
(88) Rybak-Akimova, E. V.; Masarwa, M.; Marek, K.; Warburton, P. R.; Busch, D. H. *Chem. Commun.* **1996**, 1451−1452.

(89) See Supporting Information.

smaller rate constant (k_2); it is only due to the much lower concentration of $\mathbf{1}^{\mathbf{Me_2N}}$, since the formation of species $\mathbf{3}^{\mathbf{Me_2N}}$ is proportional to the Cu(I) concentration (Figure 1, second equation). These results thus clearly reveal a significant Me_2N substituent effect; i.e., species $\mathbf{2}^{\mathbf{Me_2N}}$ has a much higher thermodynamic stability (i.e., K_1) compared to the other superoxo species $\mathbf{2}^{\mathbf{R}}$.

(d) Overall Behavior in RCN. Ligand electronic effects are manifested in the $[(L^R)Cu^I(MeCN)]^+$ ($\mathbf{1}^{\mathbf{R}}$) redox behavior (i.e., electrochemistry), CO-binding ability and in kinetics and thermodynamics of the oxygenation reactions. Relatively smaller influences for ligands with weak electron-donating abilities (L^{tBu} and L^{Me}) are due to the competitive binding of EtCN and O_2 to the copper centers, which is superimposed on the observation of intrinsic electronic effects. However, strong electron-donating groups such as MeO and Me_2N result in the observation of more significant effects on the O_2-interactions of the corresponding Cu(I)-complexes.

As noted in the Introduction, M^{III}/M^{II} reduction potentials and O_2-binding are known to relate for iron(II) and cobalt-(II) complexes;[5,60,61] linear correlations between Co^{III}/Co^{II} reduction potentials and $\log(K_{O2})$ have been observed for several series of Co(II)-complexes with different ligand systems.[66,90−92] Among these, the relationship between $\Delta E_{1/2}$ and ΔK_{O2} between complexes in a given series is quite variable, with effects seen which are greater than and smaller than what we observed for the copper systems reported here.

As we have seen, ligand electronic effects on the oxygenation reactions of $[(L^R)Cu^I(MeCN)]^+$ ($\mathbf{1}^{\mathbf{R}}$) are mostly overshadowed when the reaction is carried out in EtCN, a solvent which is also a very good ligand to Cu(I) ions. Therefore, the weakly coordinating solvents THF and acetone were used for further kinetic studies, as described in following paragraphs.

2. Oxygenation Reaction of Copper Complexes $[(L^R)Cu^I]BArF$ in THF. (a) Comparison of $[(L^H)Cu^I]^+/O_2$ Interactions in THF and EtCN. Figure 3a shows the time-dependent UV−vis spectral change for the oxygenation reaction of $[(L^H)Cu^I]^+$ in THF. The kinetic analysis shows that the behavior observed can be described by the same reaction mechanism as that determined in EtCN (cf. Figure 1). However, the reaction rates and thermodynamic stabilities of the O_2-adducts are significantly different from those in EtCN.

The rate of formation of the superoxocopper(II) complex $[(L^H)Cu^{II}(O_2^-)]^+$ ($\mathbf{2}^{\mathbf{H}}$, $\lambda_{max} = 422$ nm) in THF is faster than the stopped-flow instrumental limit of 1.3 ms ($k \geq 2 \times 10^6$ $M^{-1}s^{-1}$) even at 183 K, and only the subsequent decay of $\mathbf{2}^{\mathbf{H}}$ is observed, Figure 3a,b. Therefore, the rate constants for formation (k_1) and dissociation (k_{-1}) of species $\mathbf{2}^{\mathbf{H}}$

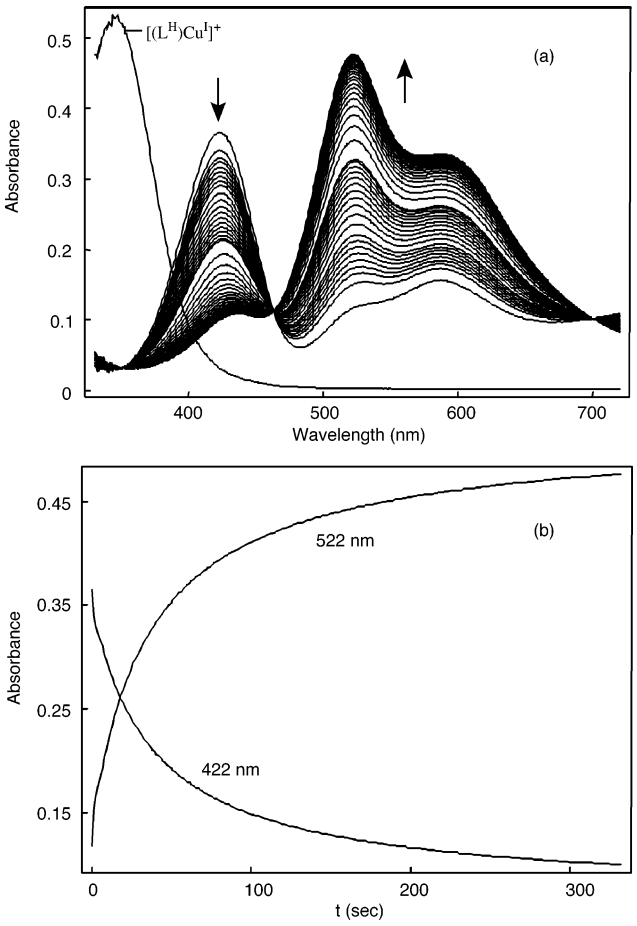

Figure 3. (a) Time-dependent UV−vis spectra for the oxygenation of $[(L^H)Cu^I]^+$ ($\mathbf{1}^{\mathbf{H}}$) in THF at 183 K. The spectrum of $[(L^H)Cu^I]^+$ ($\mathbf{1}^{\mathbf{H}}$) is also presented here for comparison. (b) Absorbance vs time at 422 nm ($[(L^H)Cu^{II}(O_2^-)]^+$, $\mathbf{2}^{\mathbf{H}}$) and 522 nm ($[\{(L^H)Cu^{II}\}_2(O_2^{2-})]^{2+}$, $\mathbf{3}^{\mathbf{H}}$) for the oxygenation of $[(L^H)Cu^I]^+$ ($\mathbf{1}^{\mathbf{H}}$) in THF at 183 K.

in THF could not be calculated, and k_1 must be at least ~100 times faster than that in EtCN (1.2×10^4 M^{-1} s^{-1} at 183 K).

However, from the temperature dependence of the spectral changes, thermodynamic parameters could be extracted, Table 4.[83] The superoxocopper(II) complex $\mathbf{2}^{\mathbf{H}}$ formed in THF is enthalpically more favored than that in EtCN ($\Delta H^\circ = -41$ kJ mol^{-1} in THF vs -29.8 kJ mol^{-1} in EtCN, Table 4). At 183 K, the equilibrium constant for formation of species $\mathbf{2}^{\mathbf{H}}$ is 2 orders of magnitude larger than that in EtCN. This is consistent with the observation that the UV−vis spectra for the oxygenation reaction (Figure 3a) lack the characteristic absorption feature for $[(L^H)Cu^I]^+$ ($\mathbf{1}^{\mathbf{H}}$) at 346 nm. At higher temperatures, the superoxocopper(II) species $[(L^H)Cu^{II}(O_2^-)]^+$ ($\mathbf{2}^{\mathbf{H}}$) in THF is destabilized by unfavorable entropic contributions, and spectral features of $\mathbf{1}^{\mathbf{H}}$ become apparent, similar to those observed in EtCN.

Data pertaining to kinetics and thermodynamics of formation of the Cu/O_2 2:1 species $[\{(L^H)Cu^{II}\}_2(O_2^{2-})]^{2+}$ ($\mathbf{3}^{\mathbf{H}}$) in THF are given in Tables 3 and 4.[83] At 183 K, the formation of peroxodicopper(II) species $\mathbf{3}^{\mathbf{H}}$ in THF (Figure 3b, 522 nm) is about 2 orders of magnitude slower than that in EtCN even though the rate constant k_2 for THF is even somewhat

(90) Harris, W. R.; McLendon, G. L.; Martell, A. E.; Bess, R. C.; Mason, M. *Inorg. Chem.* **1980**, *19*, 21−26.
(91) Kasuga, K.; Iida, Y.; Yamamoto, Y. *Inorg. Chim. Acta* **1984**, *84*, 113−116.
(92) Zanello, P.; Cini, R.; Cinquantini, A.; Orioli, P. L. *J. Chem. Soc., Dalton. Trans.* **1983**, 2159−2166.

faster (at 183 K, 1.34×10^4 in EtCN and 1.0×10^5 in THF). The rate of formation of **3^{H}** is proportional to the Cu^{I} concentration (Figure 1, second equation). However, there is very little [(L^{H})Cu^{I}]$^{+}$ (**1^{H}**) present because of the large equilibrium constant for formation (K_1) of the superoxocopper(II) species **2^{H}** in THF, as discussed already for the case of the reaction of [(L^{Me_2N})Cu^{I}]$^{+}$ (**1^{Me_2N}**) in EtCN. At higher temperatures, k_{-1} and thus the amount of **1^{H}** become more significant, and the formation rates of **2^{H}** in THF and EtCN become comparable. The dissociation (k_{-2}) of the Cu_2O_2 adduct **2^{H}** is also affected by solvent medium as reflected by a smaller k_{-2} in THF compared to that in EtCN in the temperature range that the rate constants could be determined (179−260 K).

The solvent medium has a remarkable effect on the thermodynamic stability of the 2:1 adduct **3^{H}** as indicated by a more negative reaction enthalpy in THF compared to that in EtCN, $\Delta H^\circ = -94$ kJ mol^{-1} in THF versus -77 kJ mol^{-1} in EtCN (Table 4). The overall formation constant (β) for species **3^{H}** in THF is 5 orders of magnitude larger than that in EtCN at 183 K and almost 4 orders of magnitude even at rt (Table 4).

In summary, the thermodynamic stabilities of both the 1:1 species [(L^{H})Cu^{II}(O$_2^{-}$)]$^{+}$ (**2^{H}**) and the dinuclear adduct [{(L^{H})Cu^{II}}$_2$(O$_2^{2-}$)]$^{2+}$ (**3^{H}**) are dramatically affected by the reaction medium. In THF, both the superoxo and peroxo species are more stable than in EtCN by several orders of magnitude, the latter being a binding competitor of O_2 to the copper centers. THF, although it can presumably coordinate to the metal in [(L^{R})Cu^{I}]$^{+}$ (**1**), is a weak ligand and does little to inhibit O_2-binding to copper(I).

(b) Oxygenation Reaction of [(L^{MeO})Cu^{I}]$^{+}$ in THF. As shown in Figure 4a, at 183 K the UV−vis behavior for the oxygenation reaction of [(L^{MeO})Cu^{I}]$^{+}$ (**1^{MeO}**) in THF shows remarkable differences compared to that for the unsubstituted analogue [(L^{H})Cu^{I}]$^{+}$ (**1^{H}**), Figure 3a. The formation of the superoxocopper(II) complex [(L^{H})Cu^{II}(O$_2^{-}$)]$^{+}$ (**2^{H}**) is complete within the mixing time of the stopped-flow instrument (Figure 3b), while some superoxo species **2^{MeO}** is still forming following the mixing (Figure 4b). This relatively slower formation of species **2^{MeO}** can be rationalized by the existence of a dimeric Cu(I) species ([(L^{MeO})$_2$Cu$^{I}_2$]$^{2+}$ (see description in the acetone section which follows), where disruption of the dimer structure upon dioxygen binding slows down the formation of the superoxo species. More strikingly, the transformation of the superoxo into the peroxo species is much slower for **1^{MeO}** than for **1^{H}** (Figure 4b). The concentration of the copper(I) species [(L^{MeO})Cu^{I}]$^{+}$ (**1^{MeO}**) must be minute due to a very large equilibrium constant for formation of the superoxocopper(II) complex **2^{MeO}** at 183 K. These results are indicative of a clear ligand substituent electronic effect (L^{H} vs L^{MeO}) seen in THF as solvent medium, precluding kinetic analysis at the lowest temperature.

At higher temperatures, the rate of formation of the peroxo species **3^{MeO}** strongly increases; compare Figure 5 to Figure 4a. No doubt this is again due to the shift in the equilibrium between **1^{MeO}** and **2^{MeO}**, making **1^{MeO}** available

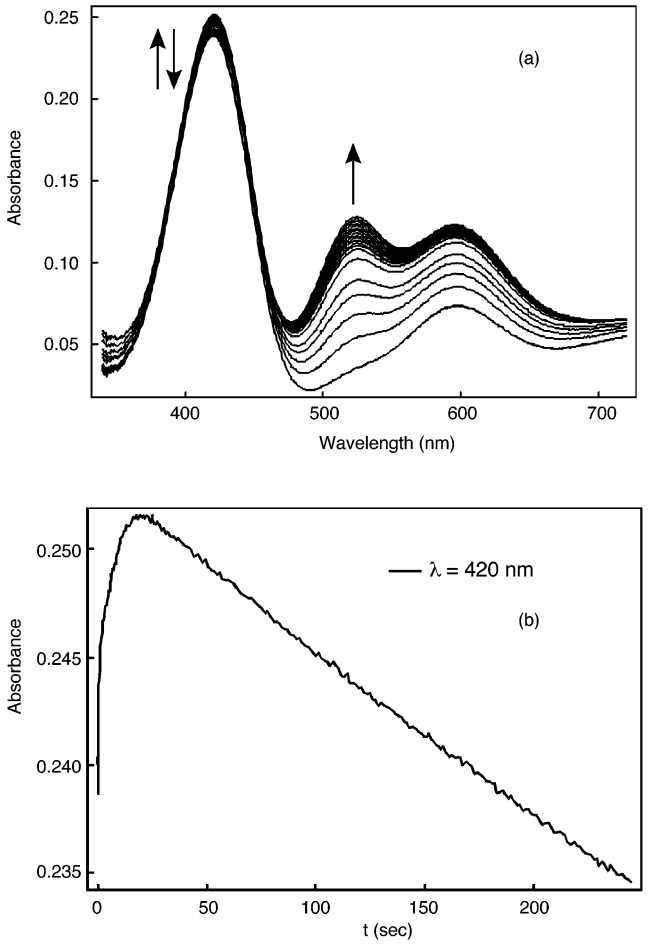

Figure 4. (a) Time-dependent UV−vis spectra for the oxygenation of [(L^{MeO})Cu^{I}]$^{+}$ (**1^{MeO}**) in THF at 183 K. (b) Absorbance vs time at 420 nm ([(L^{MeO})Cu^{II}(O$_2^{-}$)]$^{+}$, **2^{MeO}**).

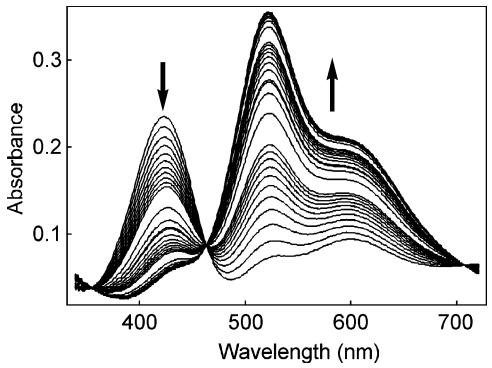

Figure 5. Time-dependent UV−vis spectra for the oxygenation of [(L^{MeO})Cu^{I}]$^{+}$ in THF at 223 K.

for the formation of the peroxo complex **3^{MeO}** (cf. Figure 1). Also, the thermodynamic stability of [{(L^{MeO})Cu^{II}}$_2$(O$_2^{2-}$)]$^{2+}$ (**3^{MeO}**) is much higher than that of [{(L^{H})Cu^{II}}$_2$(O$_2^{2-}$)]$^{2+}$ (**3^{H}**). Spectral examination (from initial spectra observed after mixing) shows that ∼80% of **3^{MeO}** is obtained even at 293 K while only ∼20% of **3^{H}** is formed. The more electron-donating ligand (L^{MeO}) significantly increases the thermodynamic stability of the corresponding peroxo species, again manifesting a considerable ligand electronic effect.

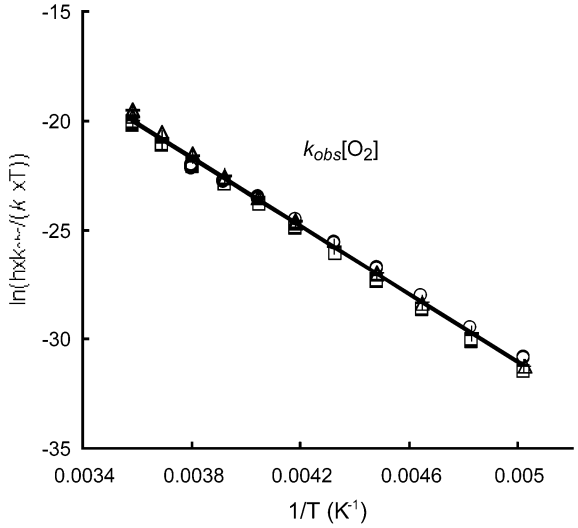

Figure 6. Eyring plots for $k_{obs}[O_2]$ pertaining to the oxygenation of $[(L^{MeO})Cu^{I}]^{+}$ in THF based on the alternative kinetic model. $[(L^{MeO})Cu^{I}]^{+}/[O_2]$: (+), 2.768 × 10^{-4} M/3.3 × 10^{-3} M; (□), 1.064 × 10^{-4} M/3.3 × 10^{-3} M; (△), 3.412 × 10^{-4} M/3.3 × 10^{-3} M; (○), 2.073 × 10^{-4} M/6.93 × 10^{-4} M.

On the basis of the general kinetic scheme shown in Figure 1, the formation rate of the peroxodicopper(II) species $\mathbf{3^{MeO}}$ is expressed by

$$d[\mathbf{3^{MeO}}]/dt = k_2[\mathbf{1^{MeO}}][\mathbf{2^{MeO}}] \quad (1)$$

As the concentration of $\mathbf{1^{MeO}}$ is too low to be experimentally determined, we can neglect k_{-2} in the rate expression, and we have to represent $\mathbf{1^{MeO}}$ as a function of the concentration of $\mathbf{2^{MeO}}$, where $[\mathbf{1^{MeO}}] = [\mathbf{2^{MeO}}]/(K_1 \cdot [O_2])$. Thus, the rate of formation of $\mathbf{3^{MeO}}$ can be rewritten as

$$d[\mathbf{3^{MeO}}]/dt = (k_2/K_1) \cdot ([\mathbf{2^{MeO}}]^2/[O_2]) \quad (2)$$

As the equilibrium constant K_1 could not be evaluated, a simplified expression was used to analyze the data.

$$2(\mathbf{2^{MeO}}) \xrightarrow{k_{obs}} \mathbf{3^{MeO}} + O_2$$

On the basis of this expression

$$d[\mathbf{3^{MeO}}]/dt = k_{obs}[\mathbf{2^{MeO}}]^2 \quad (3)$$

and along with eq 2

$$(k_2/K_1) = k_{obs}[O_2] \quad (4)$$

is derived. The Eyring plot for $k_{obs}[O_2]$ (i.e., k_2/K_1) is shown in Figure 6.

The reaction mechanism to form μ-peroxo species $[\{(L^{MeO})Cu^{II}\}_2(O_2^{2-})]^{2+}$ ($\mathbf{3^{MeO}}$) does not in fact involve an elementary step between two molecules of $\mathbf{2^{MeO}}$ (k_{obs}, eq 3). In line with the Eyring plot, Figure 7 reveals that the decay of the superoxo complex $\mathbf{2^{MeO}}$ occurs faster with air than with pure dioxygen. In order for $\mathbf{3^{MeO}}$ to form, some $\mathbf{2^{MeO}}$ must lose O_2 giving rise to $\mathbf{1^{MeO}}$, which can react with $\mathbf{2^{MeO}}$ to give the peroxo product.

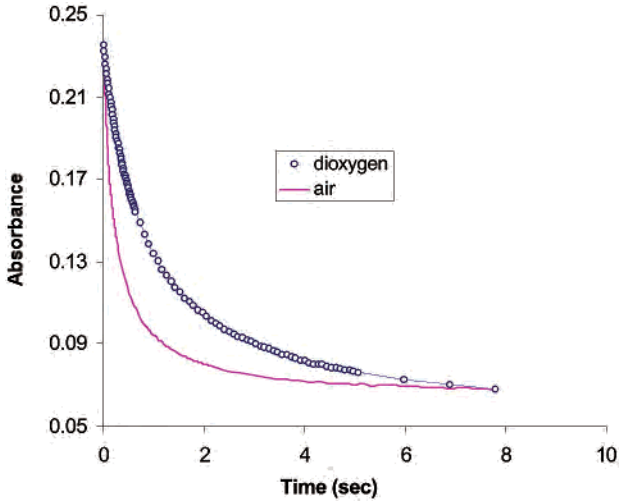

Figure 7. Absorbance vs time at 424 nm, showing the inverse $[O_2]$-dependence of the decay of $[(L^{MeO})Cu^{II}(O_2^{-})]^{+}$ ($\mathbf{2^{MeO}}$) in THF at 223 K.

Table 5. Calculated k_2/K_1 Values for Oxygenation Reactions of $\mathbf{1^H}$ and $\mathbf{1^{MeO}}$ in Both EtCN and THF Solvents

	in THF		in EtCN	
parameter	$\mathbf{1^H}$	$\mathbf{1^{MeO}}$	$\mathbf{1^H}$	$\mathbf{1^{MeO}}$
	k_2/K_1 (s^{-1})			
$\Delta H^{\ddagger}$ (kJ mol^{-1})	58.5	65.0 ± 0.4	52.5	52.38
$\Delta S^{\ddagger}$ (J K^{-1} mol^{-1})	62	66.9 ± 1.7	69.4	46.3
183 K	0.14	3.2 × 10^{-3}	18.1	1.07
223 K	1.73 × 10^2	8.4	1.26 × 10^4	6.27 × 10^2
298 K	6.48 × 10^5	7.7 × 10^4	1.73 × 10^7	1.01 × 10^6

Chemically, direct formation of the μ-peroxo species $\mathbf{3^{MeO}}$ from 2 $\mathbf{2^{MeO}}$ via a bis-superoxodicopper(II) species, $[(L)_2Cu^{II}_2(O_2^{-})_2]^{2+}$, followed by elimination of O_2, would be viable. Several bis-μ-(O_2^{-}) metal complexes have been recently characterized in detail; in fact, dioxygen evolution was observed in the decomposition processes of these bis-μ-superoxo species.[93,94] Intramolecular expulsion of O_2 would not yield an inverse $[O_2]$ dependence, however, and has to be ruled out for the ($\mathbf{L^{MeO}}$)-Cu system.

For comparison, k_2/K_1 values for the oxygenation of $\mathbf{1^H}$ in EtCN and THF as well as $\mathbf{1^{MeO}}$ in EtCN were calculated and tabulated in Table 5. The values of k_2/K_1 will reflect the relative influences of ligand or solvent on the formation (k_2)-of Cu_2O_2 adduct ($\mathbf{3^R}$) and the thermodynamic stability (K_1) of $Cu-O_2$ species ($\mathbf{2^R}$). In THF, k_2/K_1 (183 K) for L^H is ~44 times bigger than that for L^{MeO}. This suggests that in THF the ligand electronic properties have a more significant effect than in EtCN where the corresponding factor is reduced to 18. If we assume that k_2 for different substituents is nearly the same in a given solvent (cf. Table 3 for EtCN), there would be a 44-fold increase in K_1 on going form L^H to L^{MeO}. Note that the activation enthalpies for L^H and L^{MeO} are almost identical in EtCN. By contrast, in THF as solvent, the activation enthalpy (k_2/K_1) for L^{MeO} is ~6 kJ mol^{-1} higher than that for L^H, possibly attributed to a more favorable

(93) Reinaud, O. M.; Yap, G. P. A.; Rheingold, A. L.; Theopold, K. H. *Angew. Chem., Int. Ed. Engl.* **1995**, *34*, 2051−2052.
(94) Shiren, K.; Ogo, S.; Fujinami, S.; Hayashi, H.; Suzuki, M.; Uehara, A.; Watanabe, Y.; Moro-oka, Y. *J. Am. Chem. Soc.* **2000**, *122*, 254−262.

(negative) reaction enthalpy (K_1) for the formation of the superoxo species. As the temperature increases, the difference in k_2/K_1 values decreases due to entropic contributions. Again, these comparisons (of k_2/K_1) indicate that ligand electronic effects manifest themselves more strongly in THF than in EtCN, and we base this on competitive binding of EtCN to copper(I) centers.

The values of k_2/K_1 for the same ligand (L^H or L^{MeO}) can also be compared in different solvents. As shown in Table 5, the values in THF are in general smaller than those in EtCN, again manifesting a solvent effect. As indicated in Table 3, the rate constant k_2 for L^H in THF is comparable with that in EtCN. Thus, the significantly smaller value of k_2/K_1 in THF (at 183 K, 0.14 in THF vs 18.1 in EtCN, Table 5) is a result of a pronounced increase in the thermodynamic stability (K_1) of the superoxo species in THF (as given in Table 4). A smaller k_2/K_1 value was observed in THF compared with that in EtCN, for L^{MeO} also. Assuming the same expected trend for k_2, this again reflects the significantly increased thermodynamic stability of **2^{MeO}** in the less coordinating solvent.

3. Oxygenation Reaction of [(L^{R})Cu^{I}]ClO$_4$ in Acetone. A previous study[59] showed that when the oxygenation reaction of the parent complex [(L^{H})Cu^{I}]$^{+}$ (**1^{H}**) was carried out in acetone, a weakly coordinating solvent, the superoxocopper(II) species formed within the mixing time of the stopped-flow instrument and the peroxodicopper(II) complex [{(L^{H})Cu^{II}}$_2$(O$_2^{2-}$)]$^{2+}$ (**3^{H}**) exhibited enhanced rt stability compared to that generated in EtCN. But the current more detailed kinetic studies (using various L^R) show that the reaction mechanism described in Figure 1 cannot be applied for the oxygenation reaction in acetone as solvent. To analyze the kinetic results, the nature of the starting Cu(I)-complexes was studied using electrical conductivity measurements and variable-temperature ^{1}H NMR spectroscopy. The results show that they exist as dimers [(L^{R})$_2$Cu$^{I}_2$]$^{2+}$ in acetone.

Evidence for Cu(I) Dimers in Acetone Solution. Evidence for the dimeric nature of the Cu(I) complexes in acetone comes from electrical conductivity measurements and variable-temperature NMR spectroscopic studies.

(a) Conductivity Measurements. Electrical conductivity measurements[95,96] of the Cu(I) complexes were carried out in both MeCN and acetone. Onsager plots[95] for [(L^{R})$_2$Cu$^{I}_2$]$^{2+}$ complexes along with other typical but established copper-containing 1:1 and 2:1 electrolytes (see Experimental Section) are given in the Supporting Information, Figures S7−S8. The copper(I) complexes of L^R in acetone fall clearly within the family of linear plots for 2:1 electrolytes, consistent with their dimer formulations. In contrast, when conductivity measurements were carried out in MeCN, the results[89] indicate that the Cu(I) complexes are monomeric 1:1 electrolytes, suggesting that this strongly coordinating solvent breaks up the dimeric structure.

(b) Variable-Temperature NMR Studies. The ^{1}H NMR spectra of the Cu(I)-complexes in EtCN-d_5 or acetone-d_6 were recorded at variable temperature (over ∼100 K range, Figures S9−S11),[97] exhibiting very different behavior in the two solvents. In EtCN-d_5, spectra at all temperatures (185−297 K, Figure S9)[97] contain a single peak (∼4 ppm) corresponding to the hydrogen atoms from three symmetry-equivalent methylene groups connecting the amine nitrogen and the pyridine rings. A monomeric formulation, [(L^{R})Cu^{I}(MeCN)]$^{+}$ (**1^{R}**), is indicated, consistent with X-ray structures[25,76] and the conductivity data (vide supra). The broadened resonances near room temperature can be rationalized by the occurrence of the fluxional processes (i.e., involving possible dissociation and reassociation of the pyridine nitrogens) which are well-known in copper(I) complexes with nitrogen-containing ligands.[98−101] By contrast, two sets of methylene signals in a ratio of 2:1 are observed in acetone-d_6 at low temperatures (Figure S10),[97] indicating two different chemical environments for the three methylene groups. This may be rationalized by the adoption of a dimeric structure (see diagram), where each copper(I) ion is ligated with the two pyridyl nitrogens and one tertiary amine nitrogen atom of a single L^H ligand, with the fourth coordination atom from the pyridyl nitrogen of the second adjacent L^H ligand, resulting in two chemically inequivalent methylene groups. Similar splittings and temperature-dependent behavior for the methylene and 4-methoxy (CH_3O) ^{1}H-resonances are observed for **1^{MeO}** in acetone-d_6 (Figure S11).[97] The proposed dimeric structure (see diagram) is strongly suggested from the X-ray structure of the Cu(I)-complex with a similar ligand BPIA (bis((2-pyridyl)methyl)(1-methylimidazol-2-yl)methyl-((2-pyridyl)methyl)amine).[85] The dimerization of Cu(I)-complexes is furthermore well-precedented, especially when using tetradentate or tridentate nitrogen-containing ligands, such as tris(alkyl) substituted pyrazolylborates,[98,101,102] a tris-(imidazolylmethoxymethane) ligand,[96] tripodal tetradentates with oxazoline,[103] and others.[104−107] Either Cu(I)−Cu(I) interactions,[104−107] or aromatic π-stacking of ligands[108,109] (i.e., pyridine or imidazole rings) appear to facilitate the formation or stabilization of such dimers. For the copper(I) complex with BPIA ligand, a $\pi-\pi$ interaction between two pyridine rings of the two ligands in the dimer complex

(95) Geary, W. J. *Coord. Chem. Rev.* **1971**, *7*, 81−122.
(96) Sorrell, T. N.; Borovik, A. S. *J. Am. Chem. Soc.* **1987**, *109*, 4255−4260.
(97) See Supporting Information.
(98) Mealli, C.; Arcus, C. A.; Wilkinson, J. L.; Marks, T. J.; Ibers, J. A. *J. Am. Chem. Soc.* **1976**, *98*, 711−718.
(99) Jacobson, R. R. Ph.D. Thesis, State University of New York at Albany, 1989.
(100) Coggin, D. K.; Gonzalez, J. A.; Kook, A. M.; Stanbury, D. M.; Wilson, L. J. *Inorg. Chem.* **1991**, *30*, 1115−1125.
(101) Carrier, S. M.; Ruggiero, C. E.; Houser, R. P.; Tolman, W. B. *Inorg. Chem.* **1993**, *32*, 4889−4899.
(102) Hu, Z.; Williams, R. D.; Tran, D.; Spiro, T. G.; Gorun, S. M. *J. Am. Chem. Soc.* **2000**, *122*, 3556−3557.
(103) Sorrell, T. N.; Pigge, F. C.; White, P. S. *Inorg. Chim. Acta* **1993**, *210*, 87−90.
(104) Drew, M. G. B.; Lavery, A.; McKee, V.; Nelson, S. M. *J. Chem. Soc., Dalton Trans.* **1985**, 1771−1774.
(105) Gagne, R. R.; Kreh, R. P.; Dodge, J. A.; Marsh, R. E.; McCool, M. *Inorg. Chem.* **1982**, *21*, 254−261.
(106) Singh, K.; Long, J. R.; Stavropoulos, P. *Inorg. Chem.* **1998**, *37*, 1073−1079.
(107) Lee, S. W.; Trogler, W. C. *Inorg. Chem.* **1990**, *29*, 1659−1662.
(108) Wei, N.; Murthy, N. N.; Tyeklár, Z.; Karlin, K. D. *Inorg. Chem.* **1994**, *33*, 1177−1183.
(109) Bonnefous, C.; Bellec, N.; Thummel, R. P. *Chem. Commun.* **1999**, 1243−1244.

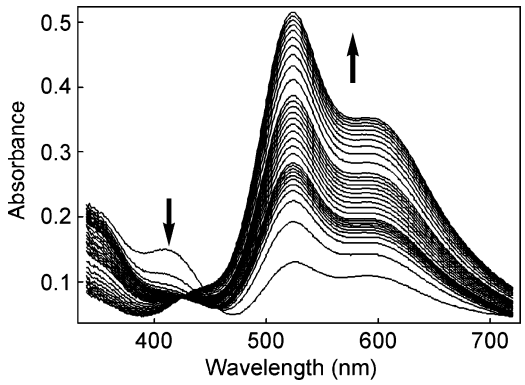

Figure 8. Time-dependent UV−vis spectra for the oxygenation of $[(L^{tBu})_2Cu^I_2]^{2+}$ in acetone at 201 K. See text for further explanations.

observed in the solid state structure is suggested to be the possible driving force for the dimerization. We suggest that the same phenomenon occurs with ligand complex $\mathbf{1^R}$ in acetone.

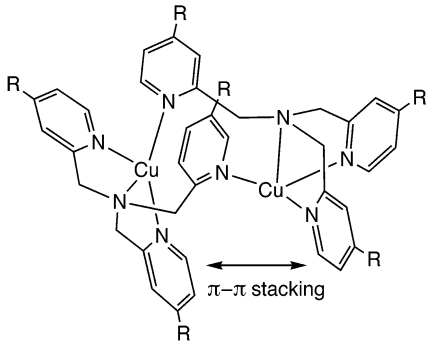

Dynamic processes for $[(L^R)Cu^I_2]^{2+}$ ($\mathbf{1^R}$) in acetone solution are indicated by the resonance broadening observed with increasing temperature (Figures S9−S11).[97] In part, because limiting (i.e., sharp) spectra were not yet observed up to room temperature, we have not attempted to analyze or determine structures or mechanisms involved in the dynamic behavior. These have been discussed elsewhere for other related systems.[101,102]

Kinetics in Acetone. With the substituted series $[(L^R)Cu^I]^+$ in hand, we carried out kinetic studies to investigate ligand electronic effects. We describe here the kinetic behavior for only the reaction of $[(L^{tBu})Cu^I]^+$ ($\mathbf{1^{tBu}}$) with dioxygen, since it could be analyzed in detail. In fact, the oxygenation reactions of $[(L^H)Cu^I]^+$ ($\mathbf{1^H}$), $[(L^{Me})Cu^I]^+$ ($\mathbf{1^{Me}}$), and $[(L^{MeO})Cu^I]^+$ ($\mathbf{1^{MeO}}$) were examined as well, qualitatively, and it was found that their overall behavior was similar, but even more complicated.[82]

The stopped-flow kinetic behavior for the oxygenation reaction of Cu(I)-complex with L^{tBu} in acetone (201 K, Figure 8) is very different from that in EtCN. A key observation is that a superoxo type species **A** with characteristic λ_{max} = 420 nm is generated within the mixing time of the instrument (∼1 ms), even at the lowest temperature (183 K). Complex **A** is not a pure superoxo species, however, since the typical Cu(I) complex absorption (λ_{max} = 340 nm) is retained at constant, i.e., concentration- and temperature-independent, proportion of roughly 50%. In line with the dimeric nature

Scheme 2

$$[(L^{tBu})_2Cu^I_2]^{2+} + O_2 \underset{k'_{-1}}{\overset{k'_1, K'_1}{\rightleftharpoons}} [(L^{tBu})_2Cu^ICu^{II}(O_2^-)]^{2+}\ (\mathbf{A})$$

$$[(L^{tBu})_2Cu^I_2]^{2+} + \mathbf{A} \xrightarrow{k'_2} [\{(L^{tBu})_2Cu^ICu^{II}\}_2(O_2^{2-})]^{4+}\ (\mathbf{B})$$

$$\mathbf{B} \xrightarrow{k'_3} \mathbf{P'}$$

$$\mathbf{P'} + O_2 \xrightarrow{\text{fast}} 2\,[\{(L^{tBu})Cu^{II}\}_2(O_2^{2-})]^{2+}\ (\mathbf{C})$$

of the initial Cu(I) species, $[(L^{tBu})_2Cu^I_2]^{2+}$, the superoxo species **A** thus is formulated as $[(L^{tBu})_2Cu^ICu^{II}(O_2^-)]^{2+}$. The assignment is further corroborated by the calculated species spectra based on kinetic analysis. The experimental data could be described assuming a second-order transformation of superoxo complex **A** into an intermediate **B**, followed by the production of the normal peroxodicopper(II) species $\mathbf{3^{tBu}}$ (**C**). As observed for the oxygenation of $[(L^{MeO})Cu^I]^+$ ($\mathbf{1^{MeO}}$) in THF, the second-order transformation of **A** into **B** also is accompanied by an inverse $[O_2]$ dependence (Figure S12),[89] indicating that 2 molecules of **A** cannot interact directly, but need fully reduced $[(L^{tBu})_2Cu^I_2]^{2+}$ present in a steady state equilibrium.

On the basis of these results, we propose a reaction mechanism, shown in Scheme 2, which involves an initial binding of dioxygen to the Cu(I) dimer at one of its two copper(I) centers to form a mixed-valence superoxocopper(II)copper(I) species $[(L^{tBu})_2Cu^ICu^{II}(O_2^-)]^{2+}$ (**A**). This reacts with a second Cu(I) dimer molecule to form a μ-peroxotetracopper species $[\{(L^{tBu})_2Cu^ICu^{II}\}_2(O_2^{2-})]^{4+}$ (**B**). Finally, intermediate **B** rearranges to the (normal) binuclear peroxodicopper(II) species **C** through an obligate intermediate **P′** (vide infra).

On the basis of the kinetics analysis, spectra for species **A**, **B**, and **C** can be calculated, and these are shown in Figure 9. The spectrum of the Cu(I)-complex, $[(L^{tBu})_2Cu^I_2]^{2+}$, is also provided in this plot for comparison. Consistent with the proposed chemistry and kinetic model, the superoxo species **A** has absorption bands at both 340 nm (characteristic of the Cu(I) moiety) and 420 nm, assigned as the superoxo-to-Cu^{II} charge-transfer band of $[(L^{tBu})_2Cu^ICu^{II}(O_2^-)]^{2+}$. The absorptivity at 420 nm (ϵ 4900 M^{-1} cm^{-1}) is in fact close to that observed for $[(L^{tBu})Cu^{II}(O_2^-)]^+$ ($\mathbf{2^{tBu}}$) in EtCN. The ratio of the Cu(I) and O_2^--complex moieties in species **A**, which is calculated by dividing the absorbance at 340 and 420 nm with the corresponding extinction coefficients, is ∼1:1, as expected for this binuclear $Cu^I\cdots Cu^{II}-O_2^-$ species (Scheme 2). The calculated spectra for the peroxo species **B** and **C** show the same absorptivities at 525 and 610 nm, which are the peroxo-to-Cu(II) charge-transfer bands, while **B** possesses significant absorption at 340 nm in addition, corresponding to the two Cu(I) moieties in the proposed tetranuclear complex $Cu^I\cdots Cu^{II}-(O_2^{2-})-Cu^{II}\cdots Cu^I$. These spectra and the kinetic analysis convincingly support the formulations of **A**, **B**, and **C**, and thus the reaction mecha-

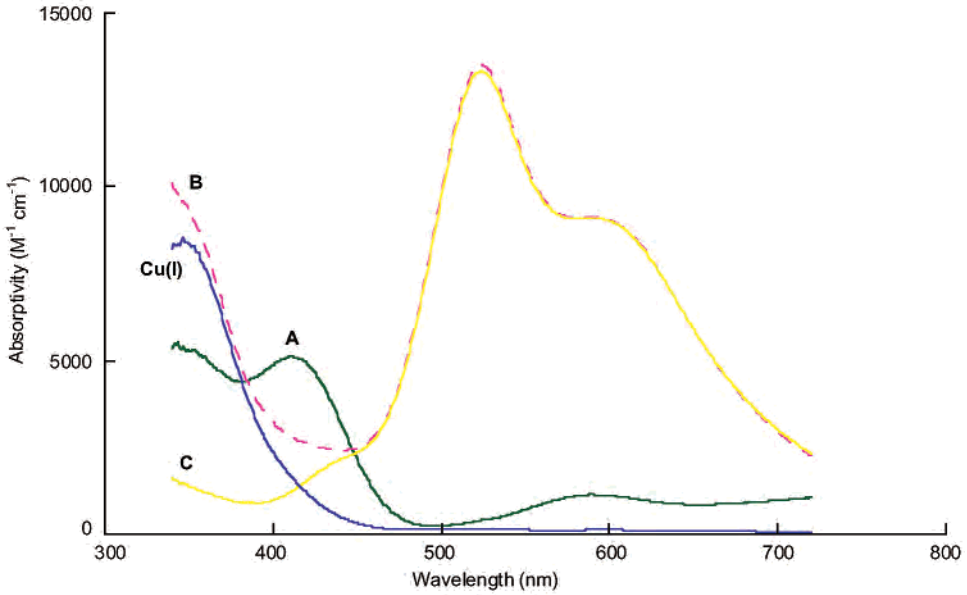

Figure 9. Calculated spectra for species **A, B**, and **C** and reference to the dicopper(I) complex starting compound, for the kinetics of reaction of O_2 with $[(L^{tBu})_2Cu^{I}_2]^{2+}$, according to Scheme 2.

Table 6. Kinetic Parameters for O_2-Interaction with $[(L^{t}Bu)_2Cu^{I}_2]^{2+}$ in Acetone

parameter	k'_2/K'_1 (s^{-1})	k'_{-1} (s^{-1})	k'_3 (s^{-1})
$\Delta H^{\ddagger}$ (kJ mol^{-1})	67.5 ± 0.6	35 ± 3	54.5 ± 0.5
$\Delta S^{\ddagger}$ (J K^{-1} mol^{-1})	112 ± 3	−95 ± 13	1 ± 2
183 K	(1.4 ± 0.1) × 10^{-1}	(5 ± 2) × 10^{-3}	(1.15 ± 0.08) × 10^{-3}
223 K	(5.1 ± 0.1) × 10^{2}	(3.8 ± 0.3) × 10^{-1}	(8.7 ± 0.1) × 10^{-1}
298 K	(6.5 ± 0.6) × 10^{6}	(6 ± 3) × 10^{1}	(1.9 ± 0.1) × 10^{3}

nism described in Scheme 2. In fact, no alternative mechanism (i.e., without dimeric **A** and/or tetrameric **B**) could be found to reasonably fit the data.

In analogy with eqs 1−2 described in the section on kinetics in THF solvent, the formation rate for species **B** can be expressed by

$$d[\mathbf{B}]/dt = k'_2[\{(L^{tBu})_2Cu^{I}_2\}^{2+}][\mathbf{A}] = k'_2[\mathbf{A}]^2/(K'_1\cdot[O_2]) \quad (5)$$

The Eyring plots for k'_2/K'_1 and k'_{-1} are given in the Supporting Information (Figure S13), obtained from data taken from 201 to 243 K for k'_2/K'_1 and from 207 to 231 K for k'_{-1}. The results are tabulated in Table 6.

According to the observed rate law, the transformation of species **B** to the normal peroxodicopper(II) species **C** is not $[O_2]$-dependent, although the reaction stoichiometry requires one molecule of dioxygen. This indicates that transformation of **B** into **C** consists of at least two steps (Scheme 2). Species **B** first rearranges (k'_3, Figure S13, 219−243 K) to a more reactive form **P′**, which might be simply an isomer of **B** or may have one of its copper(I) moieties split off from **B**. This rearrangement is the rate-determining step and exhibits no $[O_2]$ dependence. The following step(s) leading to complete transformation into species **C** are fast; neither intermediates are observed, nor are there deviations from the first-order rate law for this transformation.

Conclusion

The effects of systematic variation in ligand electronic properties on the O_2-interactions of the corresponding copper(I) complexes were investigated from the kinetic and thermodynamic aspects, utilizing a series of 4-pyridyl substituted tetradentate tripodal ligands in different solvents. We found that modification in ligand electron-donating ability can significantly affect both kinetic and thermodynamic parameters of the oxygenation reactions. The solvent also plays a crucial role in these reactions.

In EtCN, a strongly coordinating solvent, the ligand electronic effect is reduced due to the competitive binding of solvent and dioxygen to the copper centers. Thus, with weak electron-donating groups, such as Me and tBu, the kinetic and thermodynamic parameters for the formation of both the superoxocopper(II) species $[(L^{R})Cu^{II}(O_2^{-})]^{+}$ (**2^{R}**) and the peroxodicopper(II) species $[\{(L^{R})Cu^{II}\}_2(O_2^{2-})]^{2+}$ (**3^{R}**) are very similar to those for the parent complexes (i.e., R = H). But with relatively stronger electron-donating groups, utilizing ligands with MeO and Me_2N substituents, more significant effects were observed. These fall along the lines expected, as O_2-binding to cuprous ion is a redox process, favored by more reducing metal ion complexes.

When THF or acetone is used as the solvent, the formation rate for $[(L^{H})Cu^{II}(O_2^{-})]^{+}$ (**2^{H}**) is much faster than that in EtCN, suggesting the crucial role of the dissociation of the coordinated nitrile ligand in the O_2-binding process of the copper(I) complex in EtCN. For the same reason, the thermodynamic stabilities of $Cu-O_2$ species (both 1:1 and 2:1 adducts) are much higher than those in EtCN. In addition, a more significant ligand electronic effect compared to that in EtCN was observed, where the presence of electron-donating ligand L^{MeO} resulted in a pronounced increase in the thermal stability of the superoxo and peroxo species compared to that with ligand L^{H}.

When the oxygenation reactions are carried out in acetone, a different reaction mechanism involving a dimeric copper(I) species which exists in this solvent is proposed to describe the oxygenation reactions and supported by kinetic analyses.

The present study affords the first systematic investigation of both solvent medium and ligand electronic effects. Such studies are critical in the further evaluation of copper−dioxygen reactivity in biological systems, and in the design of reagents or catalysts for copper mediated oxidative chemistry.

Experimental Section

Material and Methods. Reagents and solvents used were of commercially available reagent quality unless otherwise stated. EtCN, MeCN, and heptane used for complex synthesis were distilled from CaH_2 under Ar. Diethyl ether and THF were distilled from sodium/benzophenone under Ar. Acetone was distilled from Drierite under Ar.

^{1}H NMR spectra were measured in $CDCl_3$ or CD_3NO_2 on a Bruker AMX-300 NMR spectrometer. Chemical shifts are reported as δ values downfield from an internal TMS reference. Elemental analyses were performed by Desert Analytics, Tuczon, AZ. Mass spectra were performed by the Mass Spectrometry Facility at The Johns Hopkins University.

Syntheses of Ligands and Complexes. 1. L^{tBu}. 4-*tert*-Butyl-2-picoline (4). To a stirred solution of 4-*tert*-butylpyridine (30.5 g, 0.226 mol) in freshly distilled diethyl ether (250 mL) at 195 K under Ar was added a 1.4 M diethyl ether solution of MeLi (162 mL, 0.227 mol) dropwise over 1 h. The mixture was then warmed to rt and allowed to stir overnight yielding a bright red solution. Water (∼5 mL) was added slowly to destroy residual MeLi and form LiOH as a precipitate. The resulting mixture was filtered, and the filtrate was concentrated by rotary evaporation to give a yellow oil. Purification of the crude product by vacuum distillation gave 24.3 g (72%) of a pale yellow oil. ^{1}H NMR (300 MHz, $CDCl_3$): δ 8.37 (1 H, d, J = 6 Hz), 7.12 (1H, s), 7.06 (1 H, d, J = 3 Hz), 2.53 (3 H, s), 1.28 (9 H, s).

4-*tert*-Butyl-2-picoline *N*-oxide (5). To 4-*tert*-butyl-2-picoline (24.3 g, 0.163 mol) in a 500 mL round-bottom flask was added glacial acetic acid (100 mL) along with 30% H_2O_2 (20 mL). The reaction mixture was then heated to 353 K and stirred for 12 h. The next day, more 30% H_2O_2 (20 mL) was added, and the heating was maintained for a further 12 h. After removal of the volatile components on a high-vacuum rotary evaporator, CH_2Cl_2 was added to the remaining liquid, and the residual acetic acid was neutralized with Na_2CO_3. The mixture was filtered, and the filtrate was concentrated to yield 22 g (82%) of a thick, pale, orange oil. ^{1}H NMR (300 MHz, $CDCl_3$): δ 8.18 (1H, d, J = 6 Hz), 7.21 (1H, d, J = 3 Hz), 7.12 (1H, dd, J = 6 Hz, J' = 3 Hz), 2.53 (3H, s), 1.31 (9H, s).

2-Hydroxymethyl-4-*tert*-butylpyridine (9). To 4-*tert*-butyl-2-picoline *N*-oxide (22 g, 0.133 mol) was added an excess of acetic anhydride (100 mL). The resulting mixture was heated to 383 K and stirred for 8 h. Then, after cooling to rt, the volatile components were removed by using a high-vacuum rotary evaporator. Purification of the crude product by vacuum distillation gave 9.1 g (20%) of 2-acetoxymethyl-4-*tert*-butylpyridine as a pale yellow oil. ^{1}H NMR (300 MHz, $CDCl_3$): δ 8.51 (1H, d, J = 6.0 Hz), 7.33 (1H, s), 7.26 (1H, d, J = 3.0 Hz), 5.21 (2H, s), 2.17 (3H, s), 1.32 (9H, s).

To 2-acetoxymethyl-4-*tert*-butylpyridine (9.1 g, 0.044 mol) was added NaOH (5.0 g, 0.13 mol) along with 50 mL of water. The resulting mixture was refluxed for 30 h, then cooled to rt, and extracted with ether (4 × 50 mL). The combined organic extracts were dried over Na_2SO_4, and the volatile components were removed to give 7.0 g (98%) of an orange oil. ^{1}H NMR (300 MHz, $CDCl_3$): δ 8.42 (1 H, d, J = 6.0 Hz), 7.29 (1 H, d, J = 3.0 Hz), 7.19 (1H, dd, J = 6.0 Hz, J' = 3.0 Hz), 4.78 (2 H, s), 4.34 (1H, s, br), 1.31 (9 H, s).

2-Chloromethyl-4-*tert*-butylpyridine (13). To a stirred solution of 2-hydroxymethyl-4-*tert*-butylpyridine (0.50 g, 0.0030 mol) in CH_2Cl_2 (20 mL) was added thionyl chloride (0.54 g, 0.0046 mol) slowly. After addition, the resulting mixture was stirred at rt overnight. The reaction was quenched with Na_2CO_3 aqueous solution, and the organic layer was collected. The aqueous layer was extracted with CH_2Cl_2, and the combined organic phase was dried over Na_2SO_4. Removal of volatile components gave 0.41 g (74%) of a brown liquid. R_f = 0.88 (alumina, EtOAc). ^{1}H NMR (300 MHz, $CDCl_3$): δ 8.48 (1 H, d, J = 6.0 Hz), 7.45 (1 H, d, J = 3.0 Hz), 7.24 (1H, dd, J = 6.0 Hz, J' = 3.0 Hz), 4.68 (2 H, s), 1.36 (9 H, s).

2-Phthalimidomethyl-4-*tert*-butylpyridine (17). To a stirred solution of 2-chloromethyl-4-*tert*-butylpyridine (2.47 g, 0.0133 mol) in DMF (13 mL) was added 2.47 g (0.0348 mol) of potassium phthalimide. The mixture was stirred at ∼358 K for 25 h and then cooled to rt, whereupon water (20 mL) was added and the resulting solution was extracted with $CHCl_3$ (2 × 10 mL). The organic extracts were combined and concentrated by rotary evaporation. Recrystallization from hot EtOH gave 2.6 g (81%) of a crystalline solid. ^{1}H NMR (300 MHz, $CDCl_3$): δ 8.40 (1 H, d, J = 6.0 Hz), 7.89 (2 H, m), 7.73 (2H, m), 7.28 (1 H, d, J = 3.0 Hz), 7.14 (1H, dd, J = 6.0 Hz, J' = 3.0 Hz), 4.99 (2 H, s), 1.29 (9 H, s).

2-Amino-4-*tert*-butylpyridine *bis* hydrochloride (21). To 2-phthalimidomethyl-4-*tert*-butylpyridine (2.40 g, 8.15 mmol) were added 12 M HCl (10 mL) and glacial acetic acid (10 mL). The resulting mixture was refluxed for 48 h, during which 3 aliquots of 12 M HCl (3 mL each time) were added. The reaction mixture was allowed to cool to rt, and a white crystalline solid was formed and removed by filtration. The filtrate was washed with 12 M HCl (3 × 3 mL) and then dried on a high-vacuum rotary evaporator. The resulting solid was redissolved in MeOH and layered with diethyl ether to yield 1.2 g (61%) of an off-white solid. ^{1}H NMR (300 MHz, CD_3OD): δ 8.79 (1H, d), 8.27 (1H, d), 8.10 (1H, dd), 4.5 (2H, s), 1.46 (9H, s).

L^{tBu}: (Tris[{(4-*tert*-butyl)-2-pyridyl}methyl]amine) (24). To a stirred solution of 2-aminomethyl-4-*tert*-butylpyridine bis(hydrochloride) salt (0.26 g, 0.0011 mol) and 2-chloromethyl-4-*tert*-butylpyridine (0.41 g, 0.0023 mol) in water (10 mL) was added a 1 M NaOH solution (10 mL, 0.010 mol). The reaction mixture was allowed to stir at rt overnight (the pH of the solution dropped to 7.0). The resulting solution was extracted with CH_2Cl_2 several times. The combined organic layers were dried over Na_2SO_4, and the volatile components were removed. Purification of the crude product on an alumina gel column using EtOAc as eluting solvent gave 0.30 g (60%) of a light yellow solid. ^{1}H NMR (300 MHz, $CDCl_3$): δ 8.41 (3H, d, J = 6.0 Hz), 7.70 (3H, s), 7.12 (3H, dd, J = 6.0 Hz, J' = 3.0 Hz), 3.89 (6H, s), 1.30 (27H, s). MS(FAB): m/z 459 ($M + H^+$).

[(L^{tBu})Cu^I(MeCN)](ClO_4) (1^{tBu}). To 0.16 g (0.35 mmol) of L^{tBu} and 0.11 g (0.33 mmol) of [Cu(MeCN)$_4$](ClO_4) in a 100 mL Schlenk flask was added 5 mL of deaerated CH_3CN under Ar. The resulting mixture was stirred for 30 min, and diethyl ether (50 mL) was added until a slight cloudiness developed. The solution was filtered through a coarse porosity frit, and 50 mL of diethyl ether was added to the filtrate to precipitate the complex. The supernatant was decanted, and the solid was washed with diethyl ether (2 × 50 mL). Drying in vacuo yielded 0.17 g (80%) of a bright yellow solid. ^{1}H NMR (300 MHz, CD_3NO_2): δ 7.56−7.30 (9H, s, br),

2.08 (3H, s), 1.32−1.23 (27 H, s). Anal. Calcd for $C_{32}H_{45}N_5CuClO_4$: C, 57.99; H, 6.84; N, 10.57. Found: C, 58.14; H, 6.41; N, 9.85.

2. L^{MeO}. 4-Nitro-2-picoline *N*-oxide (6). To a mixture of 2-picoline *N*-oxide (5.2 g, 0.046 mol) and 18 M H_2SO_4 (18 mL) was added fuming HNO_3 (13.8 mL) dropwise at 273 K. The resulting mixture was then heated to 373−378 K and stirred for 2 h. After cooling to rt, it was neutralized with Na_2CO_3 and extracted with CH_2Cl_2 several times. The combined organic extracts were dried over Na_2SO_4, and the volatile component was removed under vacuum to give 6.8 g (95%) of a pale yellow solid. $R_f = 0.56$ (silica, 10% MeOH−90% CH_2Cl_2). ^{1}H NMR (300 MHz, $CDCl_3$): δ 8.31 (1H, d, $J = 7.2$ Hz), 8.14 (1H, d, $J = 2.7$ Hz), 8.00 (1H, dd, $J = 7.2$ Hz, $J' = 2.7$ Hz), 2.57 (3H, s).

4-Methoxy-2-picoline *N*-oxide (7). To a solution of 4-nitro-2-picoline *N*-oxide (7.2 g, 0.047 mol) in MeOH (450 mL) was added sodium methoxide prepared from mixing 1.1 g (0.048 mol) of sodium and 150 mL of MeOH at 333 K. The resulting mixture was stirred at 333 K for 20 min and then cooled to rt, whereupon the volatile components were removed. The remaining residue was redissolved in H_2O (200 mL) and extracted with CH_2Cl_2 several times. The combined organic layers were dried over Na_2SO_4, and the volatile components were removed to give 5.5 g (84%) of light yellow liquid. $R_f = 0.35$ (silica, 10% MeOH−90% CH_2Cl_2). ^{1}H NMR (300 MHz, $CDCl_3$): δ 8.16 (1H, d, $J = 6.0$ Hz), 6.78 (1H, d, $J = 3.0$ Hz), 6.71 (1H, dd, $J = 6.0$ Hz, $J' = 3.0$ Hz), 3.84 (3H, s), 2.57 (3H, s).

2-Hydroxymethyl-4-methoxypyridine (10). To 4-methoxy-2-picoline *N*-oxide (5.4 g, 0.039 mol) was added acetic anhydride (15 mL). The resulting mixture was heated to 383 K and stirred for 4 h. After the mixture was cooled to rt, it was neutralized with a Na_2CO_3 aqueous solution and extracted with CH_2Cl_2 several times. The combined organic extracts were dried over Na_2SO_4, and the volatile components were removed. Purification of the crude product on silica gel using 4% MeOH−96% CH_2Cl_2 gave 4.2 g (60%) of 2-acetoxymethyl-4-methoxypyridine as a pale brown liquid. $R_f = 0.50$ (silica, 5% MeOH−95% CH_2Cl_2). ^{1}H NMR (300 MHz, $CDCl_3$): δ 8.46 (1H, d, $J = 6.0$ Hz), 6.92 (1H, s), 6.80 (1H, d, $J = 3.0$ Hz), 5.22 (2H, s), 3.91 (3H, s), 2.22 (3H, s).

A solution of 2-acetoxymethyl-4-methoxy-pyridine (4.2 g, 0.023 mol) in 2 N HCl aqueous solution (30 mL) was stirred at 343 K for 2 h. After the mixture was cooled to rt, it was neutralized with Na_2CO_3 and extracted with CH_2Cl_2 several times. The combined organic extracts were dried over Na_2SO_4, and the volatile components were removed. Purification of the crude product on silica gel using 5% MeOH−95% CH_2Cl_2 gave 1.9 g (60%) of a white solid. $R_f = 0.13$ (silica, 5% MeOH-95% CH_2Cl_2). ^{1}H NMR (300 MHz, $CDCl_3$): δ 8.35 (1H, d, $J = 6.0$ Hz), 6.79 (1H, d, $J = 6.0$ Hz), 6.72 (1H, dd, $J = 6.0$ Hz, $J' = 3.0$ Hz), 4.71(2H, s), 3.86 (3H, s).

2-Chloromethyl-4-methoxypyridine (14). To a stirred solution of 2-hydroxymethyl-4-methoxy-pyridine (5.0 g, 0.036 mol) in CH_2Cl_2 (150 mL) was added thionyl chloride (5.1 g, 0.043 mol) slowly. After addition, the resulting mixture was stirred at rt for 1 h. The reaction was quenched with a Na_2CO_3 aqueous solution, and the organic layer was collected. The aqueous layer was extracted with CH_2Cl_2, and the combined organic phase was dried over Na_2SO_4. Removal of volatile components gave 1.6 g (99%) of brown liquid. $R_f = 0.35$ (silica, 50% EtOAc−50% hexane). ^{1}H NMR (300 MHz, $CDCl_3$): δ 8.44 (1 H, d, $J = 6.0$ Hz), 7.05 (1 H, d, $J = 3.0$ Hz), 6.81 (1H, dd, $J = 6.0$ Hz, $J' = 3.0$ Hz), 4.93 (2 H, s), 3.93 (3 H, s).

2-Phthalimidomethyl-4-methoxypyridine (18). To a stirred solution of 2-chloromethyl-4-methoxy-pyridine (5.5 g, 0.035 mol) in DMF (60 mL) was added 6.6 g (0.035 mol) of potassium phthalimide. The mixture was stirred at ∼358 K for 72 h and then cooled to rt, and DMF was removed on a high-vacuum rotary evaporator. The remaining solid was redissolved in H_2O (100 mL), and the aqueous solution was extracted with CH_2Cl_2 several times. The organic extracts were dried over Na_2SO_4, and the volatile components were removed in vacuo. The resulting brown solid was recrystallized from hot EtOH to yield 6.6 g (71%) of a white crystalline solid. $R_f = 0.10$ (silica, 40% EtOAc−60% hexane). ^{1}H NMR (300 MHz, $CDCl_3$): δ 8.33 (1 H, d, $J = 6.0$ Hz), 7.87 (2 H, m), 7.73 (2H, m), 6.78 (1 H, d, $J = 3.0$ Hz), 6.70 (1H, dd, $J = 6.0$ Hz, $J' = 3.0$ Hz), 4.95 (2 H, s), 3.81 (3 H, s).

2-Aminomethyl-4-methoxypyridine (22). To a stirred solution of 2-phthalimidomethyl-4-methoxy-pyridine (6.6 g, 0.025 mol) in MeOH (100 mL) was added 1.8 mL (0.057 mol) of hydrazine slowly. The resulting mixture was refluxed for 3 h, and after cooling to rt, the volatile components were removed. The remaining solid was redissolved in 1 M NaOH aqueous solution (200 mL), and the solution was extracted with CH_2Cl_2 several times. The organic extracts were dried over Na_2SO_4, and the volatile component was removed in vacuo to give 3.3 g (quantitative yield) of a light yellow liquid. ^{1}H NMR (300 MHz, $CDCl_3$): δ 8.35 (1 H, d, $J = 6.0$ Hz), 6.81 (1 H, d, $J = 3.0$ Hz), 6.68 (1H, dd, $J = 6.0$ Hz, $J' = 3.0$ Hz), 3.92 (2 H, s), 3.84 (3 H, s), 1.77 (1 H, b, br).

L^{MeO}: (Tris[{(4-methoxy)-2-pyridyl}methyl]amine) (25). To a stirred solution of 2-aminomethyl-4-methoxy-pyridine (0.98 g, 0.0071mol) in CH_2Cl_2 (20 mL) were added 2-chloromethyl-4-methoxy-pyridine (2.35 g, 0.0149 mol) and 1 M NaOH solution (15 mL, 0.015 mol). The reaction mixture was stirred at 323−333 K for 96 h (the pH of the solution dropped to 7.0). The mixture was cooled to rt, the organic layer was separated, and the aqueous layer was extracted with CH_2Cl_2 several times. The combined organic layers were dried over Na_2SO_4, and the volatile components were removed. Purification of the crude product on silica gel using 3% MeOH−97% CH_2Cl_2 gave 0.95 g (35%) of a light yellow solid. ^{1}H NMR (300 MHz, $CDCl_3$): δ 8.33 (3H, d, $J = 6.0$ Hz), 7.17 (3H, d, $J = 3.0$ Hz), 6.66 (3H, dd, $J = 6.0$ Hz, $J' = 3.0$ Hz), 3.85 (6H, s), 3.84 (9H, s). High-resolution MS: *m*/*z* calcd for $C_{21}H_{24}N_4O_3$ 380.1848, found 380.1846.

[(L^{MeO})Cu^{I}(MeCN)](ClO$_4$)·0.1MeCN (1^{MeO}-(ClO$_4$)). In a 100 mL Schlenk flask equipped with a stir bar was added L^{MeO} (0.20 g, 0.52 mmol) and [Cu(MeCN)$_4$](ClO$_4$) (0.17 g, 0.52 mmol). To this mixture was added 10 mL of deaerated CH_3CN under an Ar atmosphere. The resulting bright yellow solution was stirred for 30 min. Diethyl ether (50 mL) was added to the solution until a slight cloudiness developed. The solution was filtered through a coarse frit, and 40 mL of diethyl ether was added to the filtrate to precipitate the complex. The supernatant was decanted, and the solid was washed with diethyl ether (2 × 50 mL) and dried in vacuo to yield 0.25 g (81%) of a bright yellow solid. ^{1}H NMR (300 MHz, CD_3NO_2): δ 7.04 (9H, s, br), 3.84 (9H, s), 2.00 (3.3H, s). Anal. Calcd for $C_{27}H_{27}N_5CuClO_7$·0.1MeCN: C, 47.26; H, 4.66; N, 11.98. Found: C, 47.34; H, 4.67; N, 12.01.

[Cu^{I}(L^{MeO})(MeCN)]BArF (1^{MeO}-(BArF)). To [(L^{MeO})Cu^{I}-(MeCN)](ClO$_4$) (0.11 g, 0.19 mmol) in a 100 mL Schlenk flask equipped with a stir bar was added a solution of NaBArF (0.15 g, 0.17 mmol) in 30 mL diethyl ether under Ar. The resulting solution was stirred at rt for 1 h and filtered through a coarse frit. The filtrate was collected, and the volatiles were removed under vacuum to yield 0.18 g (78%) of a yellow solid. ^{1}H NMR (300 MHz, CD_3NO_2): δ 7.84 (9H, s, br), 7.67 (4H, s), 3.91 (9H, s), 2.03 (3H,

s). Anal. Calcd for $C_{53}H_{36}N_4O_3CuBF_{24}$: C, 48.7; H, 2.78; N, 4.29. Found: C, 47.74; H, 2.63; N, 4.45.

3. L^{Me_2N}. 4-Chloro-2-picoline *N*-oxide (8). To 4-nitro-2-picoline *N*-oxide (4.0 g, 0.026 mol) in a pressure tube was added 12 M HCl aqueous solution (20 mL). After stirring at 433 K for 18 h, the reaction mixture was cooled to rt and neutralized with Na_2CO_3. The resulting aqueous solution was extracted with CH_2Cl_2 several times. The combined organic layers were dried over Na_2SO_4, and the volatile components were removed by rotary evaporation to yield 3.3 g (87%) of pale yellow liquid. $R_f = 0.5$ (silica, 10% MeOH−90% CH_2Cl_2). ^{1}H NMR (300 MHz, $CDCl_3$): δ 8.17 (1H, d, $J = 6.0$ Hz), 7.28 (1H, s), 7.15 (1H, dd, $J = 6.0$ Hz, $J' = 3.0$ Hz), 2.54 (3H, s).

To 4-chloro-2-picoline *N*-oxide (3.3 g, 0.023 mmol) was added acetic anhydride (40 mL). After refluxing at 383 K for 3 h, the reaction mixture was cooled to rt, and the volatile components were removed by using a high-vacuum rotary evaporator. Water (100 mL) was added to the remaining residue, and the resulting solution was neutralized with Na_2CO_3, which was then extracted with CH_2Cl_2 several times. The combined organic layers were dried over Na_2SO_4, and the volatile components were removed by rotary evaporation. Purification of the crude product on silica gel using 3% MeOH−97% CH_2Cl_2 gave 3.5 g (82%) of 2-acetoxymethyl-4-chloropyridine as a brown liquid. $R_f = 0.2$ (silica, 3% MeOH−97% CH_2Cl_2). ^{1}H NMR (300 MHz, $CDCl_3$): δ 8.49 (1H, d, $J = 6.0$ Hz), 7.37 (1H, d, $J = 3.0$ Hz), 7.26 (1H, dd, $J = 6.0$ Hz, $J' = 3.0$ Hz), 5.21 (2H, s), 2.20 (3H, s).

2-Hydroxymethyl-4-chloropyridine (11). To 2-acetoxymethyl-4-chloropyridine (3.5 g, 0.018 mol) was added 2 N HCl (50 mL). After stirring at 353 K for 3 h, the reaction mixture was cooled to rt and neutralized with Na_2CO_3. The resulting aqueous solution was extracted with CH_2Cl_2 several times. The combined organic layers were dried over Na_2SO_4, and the volatile components were removed by rotary evaporation to give a brown liquid. Purification of the crude product on silica gel using 5% MeOH−95% CH_2Cl_2 gave 2.3 g (85%) of a white solid. $R_f = 0.19$ (silica, 5% MeOH−95% CH_2Cl_2). ^{1}H NMR (300 MHz, $CDCl_3$): δ 8.46 (1H, d, $J = 6.0$ Hz), 7.32 (1H, d, $J = 3.0$ Hz), 7.23 (1H, dd, $J = 6.0$ Hz, $J' = 3.0$ Hz), 4.76 (2H, s), 3.56 (1H, s, br).

2-Chloromethyl-4-chloropyridine (15). To a stirred solution of 2-hydroxymethyl-4-chloropyridine (3.2 g, 0.022 mmol) in CH_2Cl_2 (200 mL) was added thionyl chloride (3.4 g, 0.029 mmol) slowly. After addition, the resulting mixture was stirred at rt for 12 h. The reaction was then quenched with Na_2CO_3 aqueous solution, and the organic layer was collected. The aqueous layer was extracted with CH_2Cl_2 several times, and the combined organic layers were dried over Na_2SO_4. Removal of volatile components gave 3.1 g (85%) of a brown liquid. $R_f = 0.71$ (silica, 10% MeOH−90% CH_2Cl_2). ^{1}H NMR (300 MHz, $CDCl_3$): δ 8.46 (1H, d, $J = 6.0$ Hz), 7.52 (1H, d, $J = 3.0$ Hz), 7.27 (1H, dd, $J = 6.0$ Hz, $J' = 3.0$ Hz), 4.66 (2 H, s).

2-Phthalimidomethyl-4-chloropyridine (**19**). To a stirred solution of 2-chloromethyl-4-chloro-pyridine (3.2 g, 0.020 mol) in DMF (60 mL) was added 3.7 g (0.035 mol) of potassium phthalimide. The mixture was stirred at ∼358 K for 48 h and then cooled to rt, and DMF was removed on a high-vacuum rotary evaporator. The remaining solid was redissolved in H_2O (100 mL), and the aqueous solution was extracted with CH_2Cl_2 several times. The organic extracts were dried over Na_2SO_4, and the volatile components were removed by rotary evaporation. The resulting brown solid was recrystallized from hot EtOH to yield 3.6 g (68%) of white crystalline solid. $R_f = 0.50$ (SiO_2, 50% EtOAc−50% hexane). ^{1}H NMR (300 MHz, $CDCl_3$): δ 8.42 (1 H, d, $J = 6.0$ Hz), 8.02 (2 H, dd, $J = 6.0$ Hz, $J' = 3.0$ Hz), 7.90 (2H, dd, $J = 6.0$ Hz, $J' = 3.0$ Hz), 7.30 (1 H, s), 7.20 (1H, dd, $J = 6.0$ Hz, $J' = 3.0$ Hz), 5.0 (2 H, s).

2-Aminomethyl-4-dimethylaminopyridine (23). To 2-phthalimidomethyl-4-chloropyridine (3.6 g, 0.013 mol) in a pressure tube were added $(CH_3)_2NH\cdot HCl$ (6.5 g, 0.080 mmol), NaOH (3.2 g, 0.080 mmol), and water (10 mL). The resulting mixture was stirred and heated to 423 K for 24 h. Following cooling to rt, water was removed by using a high-vacuum rotary evaporator. The remaining solid (**20**) was redissolved in MeOH (100 mL). To this solution was syringed in hydrazine (1.5 mL), and the resulting solution was refluxed for 3 h. The mixture was cooled to rt, and the volatile components were removed by rotary evaporation to yield brown solid which was redissolved in water (200 mL). The aqueous solution was extracted with CH_2Cl_2 several times, and the combined organic layers were dried over Na_2SO_4. Removal of the volatile components gave 2.2 g (quantitative yield) of light yellow liquid. ^{1}H NMR (300 MHz, $CDCl_3$): δ 8.16 (1H, d, $J = 6.0$ Hz), 6.48 (1H, d, $J = 3.0$ Hz), 6.38 (1H, dd, $J = 6.0$ Hz, $J' = 3.0$ Hz), 3.84 (2H, s), 3.00 (2H, s), 2.17 (2H, s, br).

2-Hydroxymethyl-4-dimethylaminopyridine (12). To 2-hydroxymethyl-4-chloropyridine (2.3 g, 0.016 mol) in a pressure tube were added $(CH_3)_2NH\cdot HCl$ (6.5 g, 0.080 mmol), NaOH (3.0 g, 0.075 mmol), and water (10 mL). The resulting mixture was stirred and heated to 423 K for 48 h and then cooled to rt, and water was removed by using a high-vacuum rotary evaporator. The remaining solid was extracted with CH_2Cl_2 several times. The combined organic layers were dried over Na_2SO_4, and the volatile components were removed by rotary evaporation to yield 2.0 g (82%) of a light brown solid. ^{1}H NMR (300 MHz, $CDCl_3$): δ 8.12 (1H, d, $J = 6.0$ Hz), 6.50 (1H, s), 6.48 (1H, m), 4.69 (2H, s), 4.44 (1H, s, br), 3.10 (6H, s).

2-Chloromethyl-4-dimethylaminopyridine (16). To a stirred solution of 2-hydroxymethyl-4-dimethylamino-pyridine (2.7 g, 0.018 mmol) in CH_2Cl_2 (150 mL) was added thionyl chloride (2.8 g, 0.023 mmol) slowly at rt. After addition, the resulting mixture was stirred at rt for 2 h. The reaction was then quenched with Na_2CO_3 aqueous solution, and the organic layer was collected. The aqueous layer was extracted with CH_2Cl_2 several times, and the combined organic layers were dried over Na_2SO_4 followed by removal of volatile components. Purification of the crude product on alumina gel using CH_2Cl_2 gave 3.0 g (99%) of a brown solid. $R_f = 0.15$ (alumina, CH_2Cl_2). ^{1}H NMR (300 MHz, $CDCl_3$): δ 8.19 (1H, d, $J = 6.0$ Hz), 6.66 (1H, d, $J = 3.0$ Hz), 6.44 (1H, dd, $J = 6.0$ Hz, $J' = 3.0$ Hz), 4.56 (2H, s), 3.03 (6H, s).

L^{Me_2N}: (Tris[(4-dimethylamino-2-pyridyl)methyl]amine) (26). To a stirred solution of 2-chloromethyl-4-dimethylamino-pyridine (1.96 g. 0.0115 mol) and 2-aminomethyl-4-dimethylamino-pyridine (0.76 g, 0.005 mol) in CH_2Cl_2 (10 mL) was added 1 N NaOH solution (15 mL). After stirring at 323−333 K for 4 days, the reaction mixture was cooled to rt, and the organic layer was separated. The aqueous layer was extracted with CH_2Cl_2 several times, and the combined organic layers were dried over Na_2SO_4. The volatile components were removed by rotary evaporation, and the remaining residue was washed with CH_3CN to yield 0.87 g (41%) of a white solid after drying in vacuo. ^{1}H NMR (300 MHz, $CDCl_3$): δ 8.14 (3H, d, $J = 6.0$ Hz), 6.98 (3H, d, $J = 3.0$ Hz), 6.35 (3H, dd, $J = 6.0$ Hz, $J' = 3.0$ Hz), 3.82 (6 H, s), 3.01 (18H, s). High-resolution MS, *m*/*z* calcd for $C_{24}H_{33}N_7$ 419.2797, found 419.2802.

[(L^{Me_2N})Cu^I]ClO_4 (1^{Me_2N}-(ClO_4)). In a 100 mL Schlenk flask equipped with a stir bar was added L^{Me_2N} (0.2 g, 0.47 mmol) and $[Cu(CH_3CN)_4](ClO_4)$ (0.15 g, 0.45 mmol). To this mixture was

added 10 mL of deaerated CH_3CN under an Ar atmosphere. The resulting bright yellow mixture was stirred for 30 min. Diethyl ether (50 mL) was added to the solution to precipitate the complex at 273 K. The supernatant was decanted, and the solid was washed with diethyl ether and dried in vacuo to yield 0.22 g (75%) of a yellow powder. ^{1}H NMR (300 MHz, CD_3NO_2): δ 7.40−6.4 (9 H, s, br), 2.98 (18 H, s). Anal. Calcd for $C_{24}H_{33}N_7CuClO_4$: C, 49.48; H, 5.71; N, 16.83. Found: C, 49.09; H, 5.54; N, 17.47.

[(L^{Me_2N})Cu^{I}]BArF (1^{Me_2N}-(BArF)). To [(L^{Me_2N})Cu^{I}](ClO$_4$) (0.12, 0.19 mmol) was added a solution of NaBArF (0.15 g, 0.17 mmol) in diethyl ether (30 mL). The resulting solution was stirred for $^1/_2$ h and filtered through a coarse frit. The volatile component was removed under vacuum, and the solid was washed with pentane and dried under vacuum to afford 0.16 g (70%) of yellow solid. ^{1}H NMR (300 MHz, CD_3NO_2): δ 7.84 (8 H, s), 7.67 (4 H, s), 2.85 (s, 9H). Anal. Calcd for $C_{56}H_{45}N_7CuBF_{24}$: C, 49.96; H, 3.37; N, 7.28. Found: C, 49.39; H, 3.37; N, 7.09.

4. L^{H}. [Cu^{I}(L^{H})]BArF·Et$_2$O (1^{H}-(BArF)). To [(L^{H})Cu^{I}(MeCN)](ClO$_4$) (0.150 g, 0.303 mmol) in a 100 mL Schlenk flask equipped with a stir bar was added a solution of NaBArF (0.268 g, 0.302 mmol) in 30 mL of diethyl ether under Ar. The resulting solution was stirred at rt for 1 h and filtered through a coarse frit. The filtrate was collected, and the volatiles were removed under vacuum to yield 0.300 g (78.9%) of a yellow solid. ^{1}H NMR (300 MHz, CD_3NO_2): δ 7.85 (9H, s, br), 7.37 (4H, s), 3.41 (4H, q), 2.07 (3H, s), 1.14 (6H, t). Anal. Calcd for for $C_{54}H_{40}N_4OCuBF_{24}$: C, 50.23; H, 3.12; N, 4.34. Found: C, 50.68; H, 3.19; N, 4.61.

5. L^{Me}. [(L^{Me})Cu^{I}(MeCN)]ClO$_4$ (1^{Me}-(ClO$_4$)). In a 100 mL Schlenk flask equipped with a stir bar was added L^{Me} (0.402 g, 1.21 mmol) and [Cu(CH$_3$CN)$_4$](ClO$_4$) (0.355 g, 1.08 mmol). To this mixture was added 10 mL of deaerated CH_3CN under an Ar atmosphere. The resulting bright yellow mixture was stirred for 30 min. Diethyl ether (50 mL) was added to the solution until the solution became cloudy. The resulting mixture was filtered, and the filtrate was collected in a 100 mL Schlenk flask. An additional 50 mL of diethyl ether was added to precipitate the complex. The supernatant was decanted, and the solid was washed with diethyl ether and dried in vacuo to yield 0.470 g (81%) of a yellow powder. ^{1}H NMR (300 MHz, CD_3NO_2): δ 7.40−6.4 (9 H, s, br), 2.98 (18 H, s). Anal. Calcd for $C_{23}H_{27}N_5CuClO_4$: C, 51.49; H, 5.07; N, 13.05. Found: C, 51.32; H, 4.90; N, 12.93.

Electrochemistry. Cyclic voltammetry was carried out using a Bioanalytical Systems BAS-100B electrochemistry analyzer. The cell consists of a modification of a standard three-chamber design equipped for handling air-sensitive solutions by utilizing high-vacuum valve seals. A platinum disk (BAS MF 2013) was used as the working electrode. The reference electrode was Ag/AgNO$_3$. The measurements were performed at rt under an Ar atmosphere in MeCN solution containing 0.1 M tetrabutylammonium hexafluorophosphate and 10^{-4}−10^{-3} M copper complex.

Conductivity Measurements. Electrical conductivity measurements were carried out in acetone using a Barnstead Sybron Corporation model PM-70CB conductivity bridge with a Yellow Springs Instrument Co. Inc. 3403 cell. The cell constant, k, was determined by using a standard aqueous KCl solution. The specific conductance, Λ, was calculated according to eq 6

$$\Lambda = 1000k(CR)^{-1} \qquad (6)$$

where R is measured resistance and C is the concentration of the sample. Studies with varying concentrations of [(L^{R})$_2$Cu$^{I}_2$]$^{2+}$ (R = H, tBu, and OMe) gave Onsager plots with straight lines having slope b = 1422 (R = H), b = 1494 (R = tBu), and b = 1390 (R = OMe). These are close to those of typical 2:1 electrolytes such as [(L^{H})Cu^{II}(H$_2$O)](ClO$_4$)$_2$[99] (b = 1477) and [Cu^{II}(XYL−O$^-$)(OH$^-$)](ClO$_4$)$_2$[110] (b = 1659), while they are very different from that of an 1:1 electrolyte [(L^{H})Cu^{II}(Cl$^-$)]ClO$_4$[111] (b = 864).

IR Spectra for CO-Adducts of the Copper(I) Complexes [(L^{R})Cu^{I}(MeCN)]$^{+}$. IR samples were prepared in a drybox by dissolving ∼35 mg of [(L^{R})Cu^{I}(MeCN)](ClO$_4$) in ∼2 mL of deaerated CH_3CN in a 10 mL Schlenk flask. Small amounts of the stock solution were transferred to a solution IR cell, and the spectra of [(L^{R})Cu^{I}(MeCN)]$^{+}$ were recorded as a control. The remaining stock solutions were bubbled with CO for ∼10 s, and the resulting solutions were transferred to a solution cell in a glovebox with a gastight syringe. The spectra were taken of the carbonylated species in order to observe the specific CO stretching frequency.

Stopped-Flow Experiments. Rapid kinetics were followed using a SFL-21 (2-mm light path/2-mL syringes) low-temperature flow unit of a SF-3A stopped-flow system (Hi-Tech Scientific) combined with a TIDAS-16 HQ/UV−vis 512/16B diode array spectrometer (J & M, 507 diodes, 300−720 nm, 1.3 ms minimum sampling time) using flexible light guides connected to a CLH-111 halogen lamp (ZEISS). The two glass coils, containing Cu(I) and dioxygen solutions, respectively, and the mixing chamber were immersed in an ethanol bath. This bath was placed in a Dewar, which was filled with liquid nitrogen for low-temperature measurements. The ethanol bath was cooled by liquid nitrogen evaporation, and its temperature was measured by using a Pt resistance thermocouple and maintained to 0.1 K by using a temperature-controlled thyristor power unit (both Hi-Tech). Concentrations of dioxygen and complex are given for rt throughout the text. For the numerical analyses, values adjusted for temperature-dependent solvent contraction were used. Dry and CO_2-free air was used instead of pure O_2 in order to vary the concentration of the latter.

Data acquisition (up to 256 complete spectra; up to 4 different time bases) was performed by using the Kinspec program (J & M). For numerical analysis, all data were pretreated by factor analysis, and concentration profiles were calculated by numerical integration using either Specfit (Spectrum Software Ass.) or Globfit (MATLAB).

The solvents EtCN and THF were dried as follows: EtCN (p.a., Merck) was predried with phosphorus pentoxide, then distilled under normal pressure, again dried using CaH_2, and redistilled immediately prior to use. THF (puriss, Merck) was dried using sodium and distilled immediately prior to use. Acetone (Uvasol, Merck) was used without further purification.

The following provides information for the kinetic studies. [(L^{H})Cu^{I}]$^{+}$ (EtCN solvent): three series, 0.17, 0.47, and 0.52 mM; 198 measurements made (179−267 K); 182 measurements used for final analysis; [O_2] = 4.4 mM; reaction time range 0.1−74 s. [(L^{Me})Cu^{I}]$^{+}$ (EtCN solvent): three series, 0.939, 0.399, and 0.269 mM; 204 measurements made (179−273 K); 202 measurements used for final analysis; [O_2] = 4.4 mM; reaction time range 0.1−195 s. [(L^{tBu})Cu^{I}]$^{+}$ (EtCN solvent): three series, 0.877, 0.502, and 0.202 mM; 210 measurements made (179−271 K); all 210 measurements used for final analysis; [O_2] = 4.4 mM; reaction time range 0.03−293 s. [(L^{MeO})Cu^{I}]$^{+}$ (EtCN solvent): three series, 0.49, 0.36, and 0.16 mM; 219 measurements made (179−297 K); 204 measurements used for final analysis; [O_2] = 4.4 mM; reaction time range 0.02−501 s. [(L^{H})Cu^{I}]$^{+}$ (THF solvent): three series, 0.26, 0.39, and 0.52 mM; 145 measurements made (183−303 K); 120 measurements used for final analysis; [O_2] = 3.3 mM; reaction

(110) Mahroof-Tahir, M. Thesis, The Johns Hopkins University, 1992.
(111) Wei, N. Ph.D. Thesis, State University of New York at Albany, 1994.

time range 0.2−751 s. $[(L^{MeO})Cu^{I}]^{+}$ (THF solvent): four series, 0.34, 0.28, and 0.11 mM (all at $[O_2] = 3.3$ mM) and 0.21 mM copper(I) complex at $[O_2] = 0.69$ mM; 158 total measurements made (175−295 K); 111 measurements used for final analysis; reaction time range 0.05−248 s. $[(L^{Me})Cu^{I}]^{+}$ (acetone solvent): one series, 0.64 mM; 47 measurements made (183−293 K); $[O_2] = 5.11$ mM; reaction time range 0.03−600 s. The complexity of the data prevented numerical analysis. $[(L^{tBu})Cu^{I}]^{+}$ (acetone solvent): two series, 0.88 mM ($[O_2] = 5.11$ mM) and 0.46 mM ($[O_2] = 0.46$ mM); 109 total measurements made (182−283 K); 54 measurements used for final analysis; reaction time range 1−142 s.

Acknowledgment. We are grateful to the National Institutes of Health (K.D.K, GM28962) and Swiss National Science Foundation (A.D.Z.) for support of this research.

Supporting Information Available: Eyring plots, van't Hoff plots, time-dependent UV−vis spectra, Onsager plots of conductivity data, variable-temperature NMR spectra, and an $[O_2]$-dependence on the kinetics of reaction, all material pertaining to the data and discussion in the main text. This material is available free of charge via the Internet at http://pubs.acs.org.

IC0205684